Principles of Microwave Imaging and Inverse Scattering

K.J. Langenberg, M. Brandfaβ, K. Mayer, T. Kreutter, A. Brüll, P. Fellinger, D. Huo

Dept. El. Eng. - University of Kassel
D-3500 Kassel, GERMANY

ABSTRACT

The heuristic imaging concept of time domain backpropagation is briefly reviewed and related to SAR. Then, algorithms based on scalar scattering theory like far-field Fourier inversion and generalized Diffraction Tomography are discussed within the framework of a unified linearization theory. Some new fundamental results concerning the information content of measurements are presented. Diffraction tomographic algorithms are then applied to electromagnetic scattering data to reveal that swept frequency or time domain experiments are completely equivalent as input data for tomographic imaging. Furthermore, an extension of linearized scalar inverse scattering to fully polarimetric linearized electromagnetic inverse scattering is presented.
Finally, an iterative solution to nonlinear, i.e. quantitative inverse scattering is discussed and illustrated with simulated data.

INTRODUCTION

Microwave imaging has applications in remote sensing of the earth, non-destructive testing of materials as well as medical diagnostics. Pertinent imaging algorithms vary from heurisitc principles (Mensa et al., 1981) to mathematically sophisticated quantitative inverse scattering (Schüller and Chaloupka, 1989; Wang and Chew, 1989; Joachimowicz et al., 1991). Recently particular concern has been given to the polarimetric information in scattering data (Boerner et al., 1992), which can either be exploited via consideration of various matrices relating the polarization of incident versus scattered field (Boerner et al., 1991; Zebker and van Zyl, 1991), or via extension of well established scalar inverse scattering schemes to the polarimetric case (Langenberg et al., 1992). In this paper, we sketch the fundamental procedure for this later approach, review linearized scalar inverse scattering, such as time domain backpropagation and diffraction tomography, and apply these algorithms in various forms to experimental data. This is an important step, because earlier experiments (Li et al., 1990) can now be made in a fully polarimetric mode (Sieber and Nesti, 1992: Blanchard et al., 1992), and, therefore, detailed knowledge about the inherent properties of presently available imaging algorithms as well as future versions (Langenberg et al., 1992; Schüller and Chaloupka, 1989; Wang and Chew, 1989; Joachimowicz et al., 1991) is required.

1. SAR IMAGING VERSUS TIME DOMAIN BACK-PROPAGATION

Usually, the Synthetic Aperture Radar (SAR) imaging scheme is understood and derived exploiting the Doppler shift of the scattered signal transmitted and received by an airborne antenna (Mensa, 1981; Harger, 1970; Wehner, 1987). Alternatively, the time domain backpropagation principle can be applied to yield mathematically the same algorithm, and, in addition, this principle can be quantitatively evaluated utilizing inverse scattering theory (Langenberg, 1987).
Let us start with a scalar wave equation (Δ is the Laplacian operator) for some potential (or scalar field component) $\Phi(\underline{\mathbf{R}}, t)$, where $\underline{\mathbf{R}}$ denotes the vector of position and t the time:

$$\Delta \Phi(\underline{\mathbf{R}}, t) - \frac{1}{c^2} \frac{\partial^2}{\partial t^2} \Phi(\underline{\mathbf{R}}, t) = -q(\underline{\mathbf{R}}, t). \tag{1}$$

Here, $q(\underline{\mathbf{R}}, t)$ is the prescribed known source where the field originates, being nonzero in a source volume V_q, and c is the wave speed. The standard retarded potential solution of (1) reads

$$\Phi(\underline{\mathbf{R}}, t) = \iiint_{V_q} \frac{q\left(\underline{\mathbf{R}}', t - \frac{|\underline{\mathbf{R}} - \underline{\mathbf{R}}'|}{c}\right)}{4\pi |\underline{\mathbf{R}} - \underline{\mathbf{R}}'|} d^3 \underline{\mathbf{R}}', \tag{2}$$

where $\underline{\mathbf{R}}'$ indicates the source point. Now we ask for the

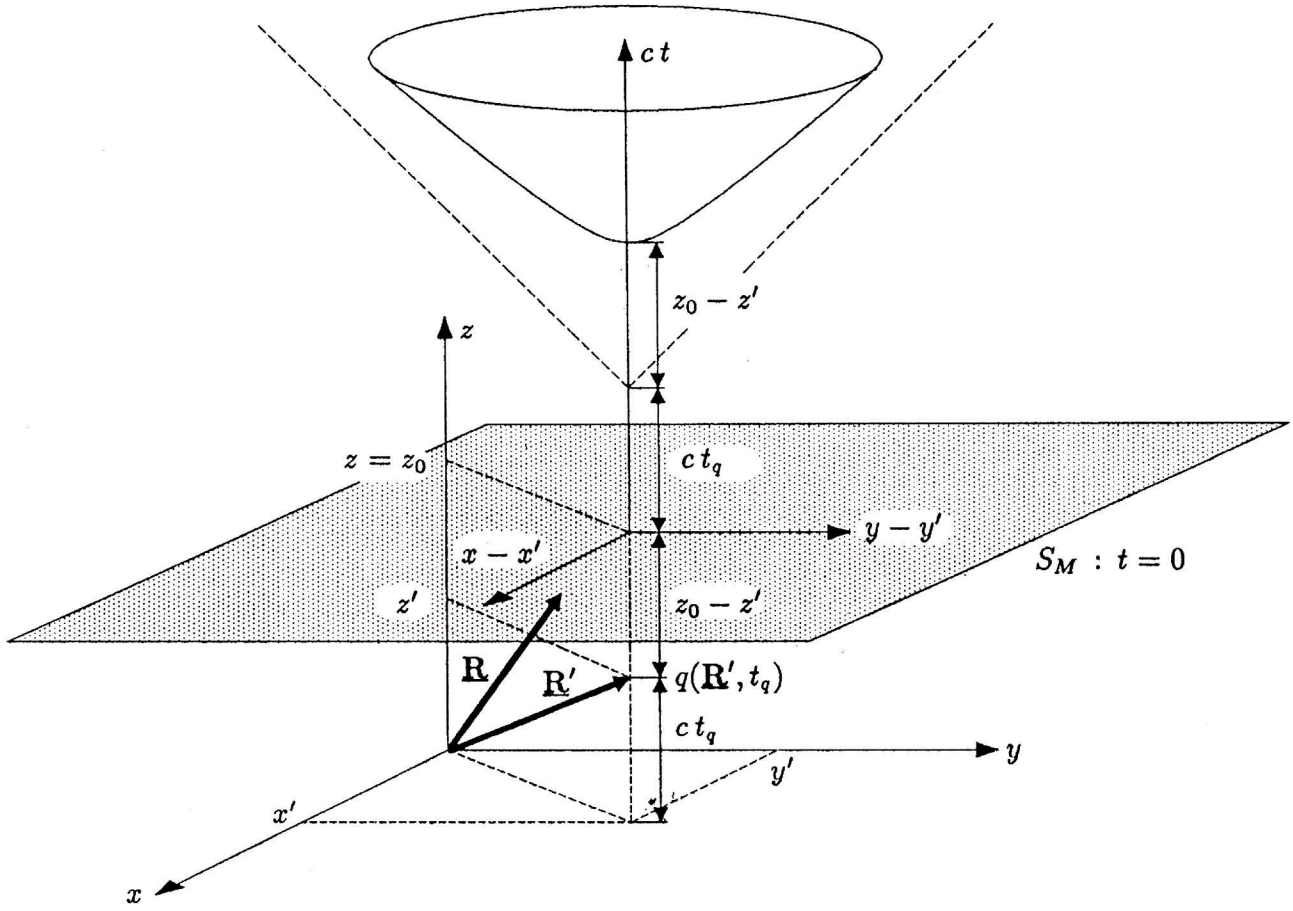

Fig. 1 - Illustration of time domain backpropagation.

set of those source points, whose source density q at time t_q contributes to the amplitude at a presribed $\underline{\mathbf{R}}$ for a fixed time t; this set is given by

$$t_q = t - \frac{|\underline{\mathbf{R}} - \underline{\mathbf{R}}'|}{c}; \tag{3}$$

reordering (3) according to

$$c\,(t - t_q) = |\underline{\mathbf{R}} - \underline{\mathbf{R}}'| \tag{4}$$

we state, that all points $\underline{\mathbf{R}}'$ on a sphere centered at $\underline{\mathbf{R}}$ with the fixed radius $c\,(t - t_q)$ contribute simultaneously at time t to the point $\underline{\mathbf{R}}$. The signal amplitude at space-time-point $\underline{\mathbf{R}}t$ has its origin in *all* source points $q\,(\underline{\mathbf{R}}', t)$ on the $\underline{\mathbf{R}}'$-sphere (4).

Instead of deriving - as above - the location of source points contributing to an $\underline{\mathbf{R}}$ t-point, we can ask the following question: which of the $\underline{\mathbf{R}}$ t-points with $\underline{\mathbf{R}} \in S_M - S_M$ denoting an appropriate measurement surface - can be reached simultaneously by a signal originating from prescribed $\underline{\mathbf{R}}'$ t_q-points? Equation (4) gives the answer; we only have to evaluate t as function of $\underline{\mathbf{R}} \in S_M$ for known t_q and $\underline{\mathbf{R}}'$. Let us specialize S_M as a plane parallel to the xy-plane of a cartesian coordinate system, in Fig. 1, with a distance z_0 from the origin. The source region V_q is supposed to reside below that plane, hence, in (2), the integration variable z' is always less than z_0. Then we have explicity instead of (4)

$$c^2\,(t - t_q)^2 - (x - x')^2 - (y - y')^2 = (z_0 - z')^2\,, \tag{5}$$

which describes in terms of the function $t\,(x\,, y)$ a so-called travel time surface, particularly a hyperboloid of revolution (compare Fig. 1). The equiphase surface of the field from a single $q\,(\underline{\mathbf{R}}'\,, t_q)$-point defocuses into such a travel time surface, and, therefore, this point should be recovered from the focusing of the measured data, i.e. from the knowledge of $\Phi\,(\underline{\mathbf{R}}\,, t)$ on S_M. This is basically the principle of the Synthetic Aperture Radar: integrate the *xyt*-data along the travel time surface for every prescribed pixel in the imaging space; whenever this pixel contains a physically real scatterer, a high amplitude is obtained; if not, only noise is displayed.

For nondestructive testing of materials with ultrasonic acoustic waves the above imaging algorithm has been adopted and termed SAFT for Synthetic Aperture Focus-

ing Technique. Experimental results for this kind of application are abundant (Schmitz et al., 1986; Langenberg 1992).

Formulated as a heurisitc principle, neither SAR nor SAFT exhibit theoretical limitations and assumptions concerning their validity; in addition, the physical meaning of the images cannot be easily established. Fortunately, when evaluated within the context of inverse scattering theory, these problems can be solved.

We have derived the time domain backpropagation imaging principle as a "solution" of the inverse source problem. In inverse scattering, equivalent sources on or inside the scatterer have to be defined, which will be pursued in the following for certain canonical classes of scatterers.

2. LINEARIZED SCALAR INVERSE SCATTERING

2.1 Definition of Equivalent Sources

Lossless dielectric and perfectly conducting scatterers provide canonical equivalent sources for microwave imaging. Let us consider the dielectric case first. This means that a certain region of space is characterized by a spatially varying wavespeed $c(\underline{\mathbf{R}})$ embedded in a medium with constant c; the volume of this region is denoted by V_c, its closed surface by S_c. The incident - illuminating - field coming from the source volume V_q is given by $\Phi_i(\underline{\mathbf{R}}, t)$, the field scattered by the spatial inhomogeneity by $\Phi_s(\underline{\mathbf{R}}, t)$. Then, after introducing a Fourier transform with regard to t according to

$$\Phi(\underline{\mathbf{R}}, \omega) = \int_{-\infty}^{\infty} \Phi(\underline{\mathbf{R}}, t)\, e^{j\omega t}\, dt, \tag{6}$$

the following differential equation for the total Fourier transformed field

$$\Phi(\underline{\mathbf{R}}, \omega) = \Phi_i(\underline{\mathbf{R}}, \omega) + \Phi_s(\underline{\mathbf{R}}, \omega) \tag{7}$$

is obtained (Herman et al., 1987)

$$\Delta\Phi(\underline{\mathbf{R}}, \omega) + k^2\Phi(\underline{\mathbf{R}}, \omega) = -q(\underline{\mathbf{R}}, \omega) - q_c^{pen}(\underline{\mathbf{R}}, \omega). \tag{8}$$

Here, $q_c^{pen}(\underline{\mathbf{R}}, \omega)$ is the equivalent source accounting for the scatterer as defined by

$$q_c^{pen}(\underline{\mathbf{R}}, \omega) = -k^2\left[1 - \frac{k^2(\underline{\mathbf{R}})}{k^2}\right]\Gamma(\underline{\mathbf{R}})\,\Phi(\underline{\mathbf{R}}, \omega), \tag{9}$$

where $k = \omega/c$ and $k(\underline{\mathbf{R}}) = \omega/c(\underline{\mathbf{R}})$ are respective wavenumbers; the upper index stands for 'penetrable'. The characteristic function

$$\Gamma(\underline{\mathbf{R}}) = \begin{cases} 1 & \text{for } \underline{\mathbf{R}} \in V_c \\ 0 & \text{for } \underline{\mathbf{R}} \notin V_c \end{cases} \tag{10}$$

constraints the equivalent source to the scattering volume V_c. Introducing the object function

$$O(\underline{\mathbf{R}}) = \left[1 - \frac{k^2(\underline{\mathbf{R}})}{k^2}\right]\Gamma(\underline{\mathbf{R}}) \tag{11}$$

we have

$$q_c^{pen}(\underline{\mathbf{R}}, \omega) = -k^2\, O(\underline{\mathbf{R}})\,\Phi(\underline{\mathbf{R}}, \omega), \tag{12}$$

which clearly exhibits the field dependence of the equivalent source. As a solution of (8) we obtain

$$\Phi(\underline{\mathbf{R}}, \omega) = \Phi_i(\underline{\mathbf{R}}, \omega) + \tag{13}$$
$$+\int_{-\infty}^{+\infty}\int_{-\infty}^{+\infty}\int_{-\infty}^{+\infty} q_c^{pen}(\underline{\mathbf{R}}', \omega)\, G(\underline{\mathbf{R}} - \underline{\mathbf{R}}', \omega)\, d^3\underline{\mathbf{R}}'$$

for the total field with $\Phi_i(\underline{\mathbf{R}}, \omega)$ given by the Fourier transform of (2); $G(\underline{\mathbf{R}} - \underline{\mathbf{R}}', \omega)$ is the scalar threedimensional free space Green function

$$G(\underline{\mathbf{R}} - \underline{\mathbf{R}}', \omega) = \frac{e^{jk|\underline{\mathbf{R}} - \underline{\mathbf{R}}'|}}{4\pi|\underline{\mathbf{R}} - \underline{\mathbf{R}}'|}. \tag{14}$$

To derive equivalent sources modeling the perfectly conducting scatterer, we recall that a twodimensional scattering problem can always be "scalarized" to a TE- or TM-problem; the pertinent boundary condition then reveals the TM-case to be a (twodimensional) Dirichlet problem, and the TE-case to be the corresponding Neumann problem. In acoustics, the Dirichelet boundary condition stands for a perfectly soft scatterer - vanishing pressure on the surface - and the Neumann boundary condition describes the perfectly rigid scatterer, which means vanishing particle displacement on the surface.

We state the Huygens-type representation for the scattered field outside V_c

$$\Phi_s(\underline{\mathbf{R}}, \omega) = \int\int_{S_c} [\,\Phi(\underline{\mathbf{R}}', \omega)\,\nabla' G(\underline{\mathbf{R}} - \underline{\mathbf{R}}', \omega) - \tag{15}$$
$$+ G(\underline{\mathbf{R}} - \underline{\mathbf{R}}', \omega)\,\nabla'\Phi(\underline{\mathbf{R}}', \omega)\,]\cdot\underline{\mathbf{n}}'\, dS',$$

where $\underline{\mathbf{n}}'$ denotes the outward normal on S_c.

Introducing the Dirichlet boundary condition $\Phi(\underline{\mathbf{R}}', \omega) \equiv 0$ for $\underline{\mathbf{R}}' \in S_c$ we have

$$\Phi_s(\underline{\mathbf{R}}, \omega) = -\int\int_{S_c} G(\underline{\mathbf{R}} - \underline{\mathbf{R}}', \omega)\,\underline{\mathbf{n}}'\cdot\nabla'\Phi(\underline{\mathbf{R}}', \omega)\, dS' \tag{16}$$

which defines an equivalent source - compare (13) -

$$q_c^s(\underline{\mathbf{R}}, \omega) = -\gamma(\underline{\mathbf{R}})\,\underline{\mathbf{n}}\cdot\nabla\Phi(\underline{\mathbf{R}}, \omega) \tag{17}$$

if we utilize the concept of the singular function $\gamma(\underline{\mathbf{R}})$ of the surface S_c according to the definition (Langenberg et al., 1992)

$$\gamma(\underline{\mathbf{R}}) = -\underline{\mathbf{n}}\cdot\nabla\Gamma(\underline{\mathbf{R}}); \tag{18}$$

The singular function has the distributional property to reduce a volume integral to a surface integral

$$\int\int\int_{V_c} \gamma(\underline{\mathbf{R}})\,\Phi(\underline{\mathbf{R}})\,d^3\underline{\mathbf{R}} = \int\int_{S_c} \Phi(\underline{\mathbf{R}})\,dS \tag{19}$$

for any appropriately given function $\Phi(\underline{\mathbf{R}})$.
The Neumann problem can be treated as follows. The boundary condition $\nabla\Phi(\underline{\mathbf{R}},\omega)\cdot\underline{\mathbf{n}} \equiv 0$ for $\underline{\mathbf{R}} \in S_c$ reduces (15) to

$$\Phi_s(\underline{\mathbf{R}},\omega) = \int\int_{S_c} \Phi(\underline{\mathbf{R}}',\omega)\,\nabla' G(\underline{\mathbf{R}}-\underline{\mathbf{R}}',\omega)\cdot\underline{\mathbf{n}}'\,dS', \tag{20}$$

which, according to (19), can be written as a volume integral

$$\Phi_s(\underline{\mathbf{R}},\omega) = \int\int\int_V \gamma(\underline{\mathbf{R}}')\,\Phi(\underline{\mathbf{R}}',\omega)\,\nabla' G(\underline{\mathbf{R}}-\underline{\mathbf{R}}',\omega)\cdot \cdot\underline{\mathbf{n}}'\,d^3\underline{\mathbf{R}}', \tag{21}$$

where $V_c \subset V$. Computing

$$\nabla\cdot(\Phi\,G\,\gamma\,\underline{\mathbf{n}}) = \gamma\,G\,\nabla\Phi\cdot\underline{\mathbf{n}} + \gamma\,\Phi\,\nabla G\cdot\underline{\mathbf{n}} + \Phi\,G\,\nabla\cdot(\gamma\,\underline{\mathbf{n}}) \tag{22}$$

we obtain instead of (21)

$$\begin{aligned}\Phi_s(\underline{\mathbf{R}},\omega) = &= \int\int\int_V \nabla'\cdot[\,\Phi(\underline{\mathbf{R}}',\omega)\,G(\underline{\mathbf{R}}-\underline{\mathbf{R}}',\omega)\,\gamma(\underline{\mathbf{R}}')\,\underline{\mathbf{n}}'\,]\,d^3\underline{\mathbf{R}} - \\ &- \int\int\int_V \gamma(\underline{\mathbf{R}}')\,G(\underline{\mathbf{R}}-\underline{\mathbf{R}}',\omega)\,\nabla'\Phi(\underline{\mathbf{R}}',\omega)\cdot\underline{\mathbf{n}}'\,d^3\underline{\mathbf{R}}' - \\ &- \int\int\int_V \Phi(\underline{\mathbf{R}}',\omega)\,G(\underline{\mathbf{R}}-\underline{\mathbf{R}}',\omega)\,\nabla'\cdot[\,\gamma(\underline{\mathbf{R}}')\,\underline{\mathbf{n}}'\,]\,d^3\underline{\mathbf{R}}'.\end{aligned} \tag{23}$$

Applying Gauss' theorem to the first volume integral in (23) we get

$$\begin{aligned}&\int\int\int_V \nabla'\cdot[\,\Phi(\underline{\mathbf{R}}',\omega)\,G(\underline{\mathbf{R}}-\underline{\mathbf{R}}',\omega)\,\gamma(\underline{\mathbf{R}}')\,\underline{\mathbf{n}}'\,]\,d^3\underline{\mathbf{R}}' = \\ &\int\int_S \Phi(\underline{\mathbf{R}}',\omega)\,G(\underline{\mathbf{R}}-\underline{\mathbf{R}}',\omega)\,\gamma(\underline{\mathbf{R}}')\,\underline{\mathbf{n}}'\cdot\underline{\mathbf{n}}'\,dS',\end{aligned} \tag{24}$$

where S is the surface of V; therefore $-\gamma(\underline{\mathbf{R}})$ being zero outside S_c - the integral (24) is zero. The remaining two integrals can be combined, and - once again exploiting the behaviour of the singular function - the region of integration can be extended to infinite space yielding

$$\begin{aligned}\Phi_s(\underline{\mathbf{R}},\omega) = -\int_{-\infty}^{+\infty}\int_{-\infty}^{+\infty}\int_{-\infty}^{+\infty} \{\,&\gamma(\underline{\mathbf{R}}')\,\nabla'\Phi(\underline{\mathbf{R}}',\omega)\cdot\underline{\mathbf{n}}' + \\ &+ \Phi(\underline{\mathbf{R}}',\omega)\,\nabla'\cdot[\,\gamma(\underline{\mathbf{R}}')\,\underline{\mathbf{n}}'\,]\}\,G(\underline{\mathbf{R}}-\underline{\mathbf{R}}',\omega)\,d^3\underline{\mathbf{R}}'.\end{aligned} \tag{25}$$

Therefore, equivalent volume sources for the Neumann boundary condition can be defined as

$$q_c^{\tau}(\underline{\mathbf{R}},\omega) = -\Phi(\underline{\mathbf{R}},\omega)\,\nabla\cdot[\,\gamma(\underline{\mathbf{R}})\,\underline{\mathbf{n}}\,] - \gamma(\underline{\mathbf{R}})\,\nabla\Phi(\underline{\mathbf{R}},\omega)\cdot\underline{\mathbf{n}} \tag{26}$$

which reduces to

$$q_c^{\tau}(\underline{\mathbf{R}},\omega) = -\Phi(\underline{\mathbf{R}},\omega)\,\nabla\cdot[\,\gamma(\underline{\mathbf{R}})\,\underline{\mathbf{n}}\,] \tag{27}$$

if the boundary condition is inserted explicitly.
In this section we have defined equivalent sources $q_c(\underline{\mathbf{R}},\omega)$ for three classes of canonical scatterers: penetrable scatterers with $q_c = q_c^{pen}$ and

$$q_c^{pen}(\underline{\mathbf{R}},\omega) = -k^2\,O(\underline{\mathbf{R}})\,\Phi(\underline{\mathbf{R}},\omega), \tag{28}$$

perfectly soft scatterers with $q_c = q_c^{s}$ and

$$q_c^{s}(\underline{\mathbf{R}},\omega) = -\gamma(\underline{\mathbf{R}})\,\underline{\mathbf{n}}\cdot\nabla\Phi(\underline{\mathbf{R}},\omega), \tag{29}$$

and, finally, perfectly rigid scatterers with $q_c = q_c^{r}$ and

$$q_c^{r}(\underline{\mathbf{R}},\omega) = -\Phi(\underline{\mathbf{R}},\omega)\,\nabla\cdot[\,\gamma(\underline{\mathbf{R}})\,\underline{\mathbf{n}}\,]. \tag{30}$$

Notice, all three equivalent sources depend upon the *total* field rendering the direct scattering as well as the inverse scattering problem nonlinear, as will be illustrated in the next section.

2.2 Nonlinearity of the Scattering and Inverse Scattering Problem

Replacing the scatterer by its pertinent equivalent source, we obtain the so-called Lippmann-Schwinger equation

$$\Phi(\underline{\mathbf{R}},\omega) = \Phi_i(\underline{\mathbf{R}},\omega) + \int\int\int_{V_c} q_c(\underline{\mathbf{R}}',\omega)\,G(\underline{\mathbf{R}}-\underline{\mathbf{R}}',\omega)\,d^3\underline{\mathbf{R}}', \tag{31}$$

which is an integral equation for the total field inside or on the scatterer, because of the field dependence of $q_c(\underline{\mathbf{R}},\omega)$. Therefore, it cannot immediately be "deconvolved" to yield the object or singula function, if, for instance, $\Phi(\underline{\mathbf{R}},\omega)$ is known *outside* the scatterer by, say, appropriate measurements.
The fact that (31) is an integral equation is the reason for the nonlinearity of the direct scattering as well as the inverse scattering problem. Let us demonstrate that for the case of a penetrable scatterer with $q_c = q_c^{pen}$ via introducing of a scattering operator

$$\boldsymbol{B}_s\{\bullet\} = -k^2\int\int\int_{V_c} O(\underline{\mathbf{R}}')\,G(\underline{\mathbf{R}}-\underline{\mathbf{R}}',\omega)\,\bullet\,d^3\underline{\mathbf{R}}' \tag{32}$$

yielding instead of (31)

$$\Phi(\underline{\mathbf{R}},\omega) = \Phi_i(\underline{\mathbf{R}},\omega) + \boldsymbol{B}_s\{\Phi(\underline{\mathbf{R}},\omega)\}. \tag{33}$$

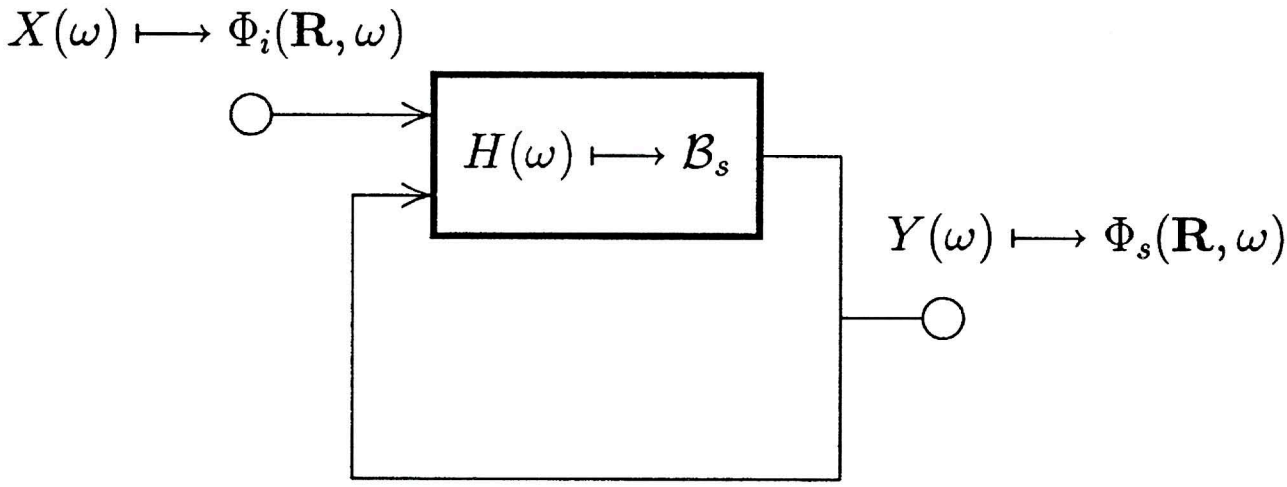

Fig. 2 - The scattering problem as an input-output feedback system.

Applying $\boldsymbol{B}_s$ to (33) we get

$$\boldsymbol{B}_s\{\Phi(\underline{\mathbf{R}},\omega)\} = \boldsymbol{B}_s\{\Phi_i(\underline{\mathbf{R}},\omega)\} + \boldsymbol{B}_s\{\boldsymbol{B}_s\{\Phi(\underline{\mathbf{R}},\omega)\}\} \quad (34)$$

or

$$(\boldsymbol{I} - \boldsymbol{B}_s)\,\boldsymbol{B}_s\{\Phi(\underline{\mathbf{R}},\omega)\} = \boldsymbol{B}_s\{\Phi_i(\underline{\mathbf{R}},\omega)\}, \quad (35)$$

where $\boldsymbol{I}$ accounts for the identity operator. The result after formal inversion of (35) reads

$$\boldsymbol{B}_s\{\Phi(\underline{\mathbf{R}},\omega)\} = (\boldsymbol{I} - \boldsymbol{B}_s)^{-1}\,\boldsymbol{B}_s\{\Phi_i(\underline{\mathbf{R}},\omega)\} \quad (36)$$

or, when compared to (33)

$$\Phi_s(\underline{\mathbf{R}},\omega) = (\boldsymbol{I} - \boldsymbol{B}_s)^{-1}\,\boldsymbol{B}_s\{\Phi_i(\underline{\mathbf{R}},\omega)\}. \quad (37)$$

Equation (37) characterizes an input-output feedback system (compare Fig. 2) with input frequency spectrum $X(\omega) = \Phi_i(\underline{\mathbf{R}},\omega)$ and output frequency spectrum $Y(\omega) = \Phi_s(\underline{\mathbf{R}},\omega)$, where the system frequancy response $H(\omega)$ is given by the scattering operator. Hence, an additive decomposition of the system into subsystems - indicating linearity - is not possible. Or, otherwise spoken, the integration over V_c which is involved in the scattering operator, cannot be separated into integrations over subvolumes of V_c.

Of course, the above nonlinearity disappears if the feedback loop is cut off. This yields instead of (37)

$$\Phi^{B}(\underline{\mathbf{R}},\omega) = \Phi_i(\underline{\mathbf{R}},\omega) + \boldsymbol{B}_s\{\Phi_i(\underline{\mathbf{R}},\omega)\} \quad (38)$$

for $\underline{\mathbf{R}} \notin V_c$; together with approximation $\Phi(\underline{\mathbf{R}},\omega) = \Phi_i(\underline{\mathbf{R}},\omega)$ for $\underline{\mathbf{R}} \in V_c$ this linearization is known as the Born approximation, whence the upper index. Obviously, it requires something like a weak scatterer (Keller, 1969).

Linearizations can also be invented for the other two classes of canonical scatterers. They are associated with the name of Kirchhoff, and, in principal, the total field on the scattering surface is once more related to the incident field alone. The argument follows so-called physical optics; we will come back to it in the section on linearized polarimetric imaging. But notice, linearization is mandatory as soon as the output of time domain backpropagation (or frequency diversity generalized diffraction tomography) should be quantitatively discussed. In addition, the incident field has also to be specified in order to end up with applicable algorithms; in general, bistatic arrangements require a plane wave approximation, whereas monostatic setups induce a point transmitter-receiver.

2.3 Frequency Diversity Generalized Diffraction Tomography

2.3.1 Generalized Holographic Field and Porter-Bojarski Integral Equation

Suppose the scatterer resides within an arbitrarly closed measurement surface S_M defining a volume $V_M \supset V_c$; suppose further that the measurements comprise the field $\Phi(\underline{\mathbf{R}},\omega)$ as well as its normal derivative on S_M. We then have as appropriate representation of the scattered field *outside* V_M in terms of the Huygens integral

$$\Phi_s(\underline{\mathbf{R}},\omega) = \int\int_{S_M} [\,\Phi(\underline{\mathbf{R}}',\omega)\,\nabla' G(\underline{\mathbf{R}} - \underline{\mathbf{R}}',\omega) - \\ + G(\underline{\mathbf{R}} - \underline{\mathbf{R}}',\omega)\,\nabla'\Phi(\underline{\mathbf{R}}',\omega)\,]\cdot\underline{\mathbf{n}}'\,dS'. \quad (39)$$

Unfortunately, for points $\underline{\mathbf{R}}$ *inside* V_M the integral (39) yields only $-\Phi_i(\underline{\mathbf{R}},\omega)$, and, therefore, tells nothing about the field in the scattering region. R. Porter and N. Bojarski independently proposed (Porter, 1970; Bojarski, 1981) to replace (39) by

$$\Theta_H(\underline{\mathbf{R}},\omega) = -\int\int_{S_M} [\,\Phi_s(\underline{\mathbf{R}}',\omega)\,\nabla' G^*(\underline{\mathbf{R}}-\underline{\mathbf{R}}',\omega) -$$

$$+ G^*(\underline{\mathbf{R}}-\underline{\mathbf{R}}',\omega)\,\nabla'\Phi(\underline{\mathbf{R}}',\omega)\,]\cdot\underline{\mathbf{n}}'\,dS' \qquad (40)$$

for points $\underline{\mathbf{R}}$ inside V_M which defines the so-called generalized holographic field $\Theta_H(\underline{\mathbf{R}},\omega)$ via backpropagation of the measurements, whence the complex conjugate of Green's function as indicated by the upper *. Applying Green's theorem to the interior of S_M and recognizing

$$\Delta\,\Phi_s(\underline{\mathbf{R}},\omega) + k^2\,\Phi_s(\underline{\mathbf{R}},\omega) = -\,q_c(\underline{\mathbf{R}},\omega) \text{ for } \underline{\mathbf{R}}\in V_M \qquad (41)$$

we obtain the Porter-Bojarski integral equation for $\underline{\mathbf{R}}\in V_M$

$$\Theta_H(\underline{\mathbf{R}},\omega) = \qquad (42)$$

$$= 2j\int_{-\infty}^{+\infty}\int_{-\infty}^{+\infty}\int_{-\infty}^{+\infty} q_c(\underline{\mathbf{R}}',\omega)\,G_i(\underline{\mathbf{R}}-\underline{\mathbf{R}}',\omega)\,d^3\,\underline{\mathbf{R}}',$$

where the imaginary part of G is involved as kernel. Due to the compact support of q_c we have been able to extend the integration limits to infinity. Notice, (42) has a computable inhomogeneity, hence, we have an integral equation of the first kind for the unknown equivalent sources. Before we discuss its solution, we give a somewhat different definition of generalized holographic field $\psi_H(\underline{\mathbf{R}},\omega)$, which seems more appropriate for the application of spatial Fourier transforms:

$$\psi_H(\underline{\mathbf{R}},\omega) = \int\int_{S_M} [\,\Phi_s(\underline{\mathbf{R}}',\omega)\,\nabla' G_i(\underline{\mathbf{R}}-\underline{\mathbf{R}}',\omega) - \qquad (43)$$

$$+ G_i(\underline{\mathbf{R}}-\underline{\mathbf{R}}',\omega)\,\nabla'\Phi_s(\underline{\mathbf{R}}',\omega)\,]\cdot\underline{\mathbf{n}}'\,dS'.$$

This definition results in the same Porter-Bojarski equation for $\Psi_H(\underline{\mathbf{R}},\omega)$ for points $\underline{\mathbf{R}}$ either *inside* or *outside* S_M which differs from (42) by omission of the factor $2j$. In addition, it makes (43) amenable to a threedimensional spatial Fourier transform. We have the relationship:

$$2j\,\psi_H(\underline{\mathbf{R}},\omega) = \begin{cases}\Theta_H(\underline{\mathbf{R}},\omega) & \text{for } \underline{\mathbf{R}} \text{ inside } S_M\\ \Theta_H(\underline{\mathbf{R}},\omega) + \Phi_s(\underline{\mathbf{R}},\omega) & \text{for } \underline{\mathbf{R}} \text{ outside } S_M\end{cases}. \qquad (44)$$

Trying to solve the Porter-Bojarski integral equation we have to cope with two problems

- The equivalent source comprises *two* unknows, the object (singular) function and the total field. A remedy concerns linearization with either the Born or Kirchhoff approximation, together with a specification of the incident field.
- The generalized holographic field is rather pathological in the sense that its threedimensional spatial Fourier transform is only nonzero on a sphere of radius k in Fourier space, which is called the Ewald sphere. Therefore, it provides only minimal norm information about the equivalent sources. The remedy is diversity together with a specification of the incident field, resulting in either frequency or angular diversity. To apply diversity, linearization is once more mandatory.

As a matter of fact, the second one of the above items has its origin in the structure of the threedimensional spatial Fourier transform of the imaginary part of Green's function, being defined as

$$\tilde{G}_i(\underline{\mathbf{K}},\omega) = \int_{-\infty}^{+\infty}\int_{-\infty}^{+\infty}\int_{-\infty}^{+\infty} G_i(\underline{\mathbf{R}},\omega)\,e^{-j\underline{\mathbf{K}}\cdot\underline{\mathbf{R}}}\,d^3\,\underline{\mathbf{R}}. \qquad (45)$$

Since $G_i(\underline{\mathbf{R}},\omega)$ satisfies a homogeneous Helmholtz equation

$$\Delta\,G_i(\underline{\mathbf{R}},\omega) + k^2\,G_i(\underline{\mathbf{R}},\omega) = 0, \qquad (46)$$

we obtain by application of the Fourier transform (45) - it is $K = |\,\underline{\mathbf{K}}\,|$ -

$$(K^2 - k^2)\,\tilde{G}_i(\underline{\mathbf{K}},\omega) = 0 \qquad (47)$$

with the general- distributional- solution

$$\tilde{G}_i(\underline{\mathbf{K}},\omega) = G_0(\omega)\,\delta(K^2 - k^2), \qquad (48)$$

where $G_0(\omega)$ denotes an arbitrary amplitude function. The inverse Fourier transform yields

$$G_i(\underline{\mathbf{R}},\omega) = \text{sign}(k)\,\frac{G_0(\omega)}{4\pi^2}\,\frac{\sin k\,R}{R} \qquad (49)$$

with the signum function defined by

$$\text{sign}(k) = \begin{cases}-1 \text{ for } k<0\\ 1 \text{ for } k>0\end{cases}.$$

Now, applying the above procedure to the real part $G_r(\underline{\mathbf{R}},\omega)$ of $G(\underline{\mathbf{R}},\omega)$, i.e. transforming the differential equation

$$\Delta\,G_r(\underline{\mathbf{R}},\omega) + k^2\,G_r(\underline{\mathbf{R}},\omega) = -\,\delta(\underline{\mathbf{R}}) \qquad (50)$$

to find the solution in $\underline{\mathbf{K}}$-space (Fourier space)

$$\tilde{G}_r(\underline{\mathbf{K}},\omega) = \frac{1}{(K^2 - k^2)} \qquad (51)$$

we get via inverse spatial Fourier transform

$$G_r(\underline{\mathbf{R}},\omega) = \frac{\cos k\,R}{4\pi R}, \qquad (52)$$

and, hence, (49) is the pertinent imaginary part - pertinent in the sense, that the *time domain* Green function $G(\underline{\mathbf{R}},t)$ is causal - to be conmbined with the real part (52) if and only if

$$G_0(\omega) = \pi\,\text{sign}(k). \qquad (53)$$

Therefore we finally have

$$\tilde{G}_i(\underline{\mathbf{K}}, \omega) = \pi \operatorname{sign}(k)\, \delta(K^2 - k^2) \tag{54}$$

yielding the following Fourier transformed Porter-Bojarski equation

$$\tilde{\psi}_H(\underline{\mathbf{K}}, \omega) = \pi \operatorname{sign}(k)\, \tilde{q}_c(\underline{\mathbf{K}}, \omega)\, \delta(K^2 - k^2)\,. \tag{55}$$

We state that the generalized holographic field $\psi_H(\underline{\mathbf{R}}, \omega)$ contains only information about the Fourier spectrum of the equivalent sources on the Ewald sphere $K = k$.

In the following we want to show explicity that, in fact, the Fourier transformed generalized holographic field is identically zero outside the Ewald sphere; *on* the Ewald sphere it is related to appropriately defined measurements. Noticing

$$\iint_{S_M} [\, \Phi_i(\underline{\mathbf{R}}', \omega)\, \nabla' G_i(\underline{\mathbf{R}} - \underline{\mathbf{R}}', \omega) - \\ + G_i(\underline{\mathbf{R}} - \underline{\mathbf{R}}', \omega)\, \nabla' \Phi_i(\underline{\mathbf{R}}', \omega)\,] \cdot \underline{\mathbf{n}}'\, dS' = 0 \tag{56}$$

on behalf of Green's theorem, we can equally define instead of (43)

$$\psi_H(\underline{\mathbf{R}}, \omega) = \iint_{S_M} [\, \Phi(\underline{\mathbf{R}}', \omega)\, \nabla' G_i(\underline{\mathbf{R}} - \underline{\mathbf{R}}', \omega) - \\ + G_i(\underline{\mathbf{R}} - \underline{\mathbf{R}}', \omega)\, \nabla' \Phi(\underline{\mathbf{R}}', \omega)\,] \cdot \underline{\mathbf{n}}'\, dS'\,. \tag{57}$$

Taking the spatial Fourier transform of this equation results in

$$\tilde{\psi}_H(\underline{\mathbf{K}}, \omega) = \tilde{G}_i(\underline{\mathbf{K}}, \omega)\, \tilde{M}(\underline{\mathbf{K}}, \omega) \tag{58}$$

with

$$\tilde{M}(\underline{\mathbf{K}}, \omega) = \\ \iint_{S_M} \left[\Phi(\underline{\mathbf{R}}', \omega) \nabla' e^{-j\underline{\mathbf{K}} \cdot \underline{\mathbf{R}}'} - \nabla' \Phi(\underline{\mathbf{R}}', \omega)\, e^{-j\underline{\mathbf{K}} \cdot \underline{\mathbf{R}}'} \right] \cdot \underline{\mathbf{n}}' dS' \tag{59}$$

By introducing the singular function $\gamma_{S_M}(\underline{\mathbf{R}})$ of the measurement surface, (59) transforms into

$$\tilde{M}(\underline{\mathbf{K}}, \omega) = \int_{-\infty}^{+\infty} \int_{-\infty}^{+\infty} \int_{-\infty}^{+\infty} \gamma_{S_M}(\underline{\mathbf{R}}') \\ \left[\Phi(\underline{\mathbf{R}}', \omega)\, \nabla' e^{-j\underline{\mathbf{K}} \cdot \underline{\mathbf{R}}'} - \nabla' \Phi(\underline{\mathbf{R}}', \omega)\, e^{-j\underline{\mathbf{K}} \cdot \underline{\mathbf{R}}'} \right] \cdot \underline{\mathbf{n}}' d^3 \underline{\mathbf{R}}' \tag{60}$$

or

$$\tilde{M}(\underline{\mathbf{K}}, \omega) = \\ -j\underline{\mathbf{K}} \cdot \int_{-\infty}^{+\infty} \int_{-\infty}^{+\infty} \int_{-\infty}^{+\infty} \gamma_{S_M}(\underline{\mathbf{R}}')\, \underline{\mathbf{n}}'\, \Phi(\underline{\mathbf{R}}', \omega)\, e^{-j\underline{\mathbf{K}} \cdot \underline{\mathbf{R}}'} d^3 \underline{\mathbf{R}}' - \\ - \int_{-\infty}^{+\infty} \int_{-\infty}^{+\infty} \int_{-\infty}^{+\infty} \gamma_{S_M}(\underline{\mathbf{R}}')\, \underline{\mathbf{n}}' \cdot \nabla' \Phi(\underline{\mathbf{R}}', \omega)\, e^{-j\underline{\mathbf{K}} \cdot \underline{\mathbf{R}}'} d^3 \underline{\mathbf{R}}'\,. \tag{61}$$

The integrals in (61) are obviously threedimensional Fourier integrals enabling us to transform $\tilde{M}(\underline{\mathbf{K}}, \omega)$ into the spatial domain according to

$$M(\underline{\mathbf{R}}, \omega) = -\nabla \cdot [\, \gamma_{S_M}(\underline{\mathbf{R}})\, \underline{\mathbf{n}}\, \Phi(\underline{\mathbf{R}}, \omega)\,] - \gamma_{S_M}(\underline{\mathbf{R}})\, \underline{\mathbf{n}} \cdot \\ \cdot \nabla \Phi(\underline{\mathbf{R}}, \omega)\,. \tag{62}$$

Defining equivalent Dirichlet and Neumann type sources in terms of the field on the measurement surface*, i.e. according to (29) and (26)

$$q^D_{S_M}(\underline{\mathbf{R}}, \omega) = -\gamma_{S_M}(\underline{\mathbf{R}})\, \underline{\mathbf{n}} \cdot \nabla \Phi(\underline{\mathbf{R}}, \omega) \tag{63}$$

$$q^N_{S_M}(\underline{\mathbf{R}}, \omega) = -\Phi(\underline{\mathbf{R}}, \omega) \nabla \cdot [\, \gamma_{S_M}(\underline{\mathbf{R}})\, \underline{\mathbf{n}}\,] - \gamma_{S_M}(\underline{\mathbf{R}})\, \underline{\mathbf{n}} \cdot \\ \cdot \nabla \Phi(\underline{\mathbf{R}}, \omega) \tag{64}$$

we find by comparison with (62)

$$M(\underline{\mathbf{R}}, \omega) = q^N_{S_M}(\underline{\mathbf{R}}, \omega) + q^D_{S_M}(\underline{\mathbf{R}}, \omega) \tag{65}$$

This equation is a very intuitive and useful way to characterize measurements mathematically. Equation (58) tells us

$$\tilde{\psi}_H(\underline{\mathbf{K}}, \omega) = \pi \operatorname{sign}(k)\, \tilde{M}(\underline{\mathbf{K}}, \omega)\, \delta(K^2 - k^2) \tag{66}$$

yielding when compared to (55)

$$\tilde{M}(\underline{\mathbf{K}}, \omega)\, \delta(K^2 - k^2) = \tilde{q}_c(\underline{\mathbf{K}}, \omega)\, \delta(K^2 - k^2)\,. \tag{67}$$

This is just another version of the Porter-Bojarski equation; from it, we either deduce

$$M(\underline{\mathbf{R}}, \omega) \bigstar G_i(\underline{\mathbf{R}}, \omega) = q_c(\underline{\mathbf{R}}, \omega) \bigstar G_i(\underline{\mathbf{R}}, \omega)\,, \tag{68}$$

where the star indicates threediomensional convolution with regard to $\underline{\mathbf{R}}$, or, equivalently

$$\tilde{M}(\underline{\mathbf{K}} = k\,\hat{\underline{\mathbf{K}}}, \omega) = \tilde{q}_c(\underline{\mathbf{K}} = k\,\hat{\underline{\mathbf{K}}}, \omega)\,. \tag{69}$$

Hence, a complete set of measurements on S_M made for a single frequency and a single incident field only provides Ewald sphere information about $q_c(\underline{\mathbf{R}}, \omega)$ - at least within the context of the Porter-Bojarski equation. But, as we deduce from the Huygens representation (15) of the field outside S_M, this complete set of measurements fully determines that field, and, therefore, nothing is won measuring $\Phi_s(\underline{\mathbf{R}}, \omega)$ in some finite measurement *volume*. We conclude that diversity in either frequency or in another appropriate parameter of the incident field - like the angle of incidence of an illuminating plane wave - is mandatory in order not to stay with the minimal norm solution (69) of generalized holography itself. Examples for such minimal norm solutions are given in (Herman et al., 1987) and they clearly illustrate, that there is no quantitative solution to the inverse scattering problem - neither linearized nor

* Notice, the field does not necessarily satisfy *any* boundary condition on S_M, hence, neither $\Phi(\underline{\mathbf{R}}, \omega)$ nor $\underline{\mathbf{n}} \cdot \nabla \Phi(\underline{\mathbf{R}}, \omega)$ must be zero on S_M.

normalized - for a single frequency and a single illumination angle, as it is sometimes claimed in the literature (Caorsi et al., 1991).

2.3.2 Frequency Integration of the Porter-Bojarski Integral Equation

In microwave imaging one has easy access to frequency diversity making phase coherent measurements over a wide frequency range. Therefore, we discuss only the frequency integration of the Porter-Bojarski integral equation and leave the reader to the literature for the angular diversity case (Herman et al., 1987; Porter, 1986) and for the "all the data" case (Oristaglio, 1989).

Let us illustrate why a straightforward solution of the Porter- Bojarsky equation requires linearization. In Fig. 3 the $(K_x K_y) K_z$-plane represent $\underline{\mathbf{K}}$-space (in cartesian coordinates), and the k-axis refers to frequency diversity. The circles indicate Ewald "spheres" for two different frequencies, and clearly, choosing the frequencies ω_1 we obtain an equivalent source $q_c^{(1)}(\underline{\mathbf{K}} = k_1 \hat{\underline{\mathbf{K}}}, \omega_1)$, whereas the choice of ω_2 *changes* $q_c^{(1)}$ to $q_c^{(2)}(\underline{\mathbf{K}} = k_2 \hat{\underline{\mathbf{K}}}, \omega_2)$ i.e. to apply frequency diversity we have to control the frequency dependence of the equivalent source. This is possible if we linearize with either the Born or Kirchhoff approximation.

We consider the penetrable scatterer for the "bistatic" plane wave incident field

$$\Phi_i(\underline{\mathbf{R}}, \omega) = F(\omega)\, e^{jk\hat{\mathbf{k}}_i \cdot \underline{\mathbf{R}}}, \tag{70}$$

i.e. with a fixed unit-vector of propagation $\hat{\mathbf{k}}_i$; $F(\omega)$ denotes the frequency spectrum of the transmitted signal, be it either for a swept frequency or a pulsed experiment. The case of a point- source excitation is treated in (Esmersoy et al., 1985) in a somewhat different way. Then we have within the Born approximation - recall the definition of $O(\underline{\mathbf{R}})$ in (11) -

$$q_c^{pen,B}(\underline{\mathbf{R}}, \omega) = -k^2 F(\omega)\, O(\underline{\mathbf{R}})\, e^{jk\hat{\mathbf{k}}_i \cdot \underline{\mathbf{R}}}. \tag{71}$$

Real time domain signals only require consideration $\omega \geq 0$ because negative frequencies are occupied by the complex conjugate spectral values if three residing for $\omega \geq 0$; we then have instead of (55)

$$\tilde{\psi}_H(\underline{\mathbf{K}}, \omega) = \frac{\pi}{2k}\, \tilde{q}_c^{pen,B}(\underline{\mathbf{K}}, \omega)\, \delta(K - k). \tag{72}$$

Inserting (71) and integrating with regard to frequancy yields (Herman et al., 1987)

$$O(\underline{\mathbf{R}}) = -\frac{1}{\pi}\, \Re\left\{ \int_0^\infty \frac{1}{k^2 F(\omega)}\, \hat{\mathbf{k}}_i \cdot \nabla\left[\Theta_H(\underline{\mathbf{R}}, \omega)\, e^{-jk\hat{\mathbf{k}}_i \cdot \underline{\mathbf{R}}} \right] dk \right\} \tag{73}$$

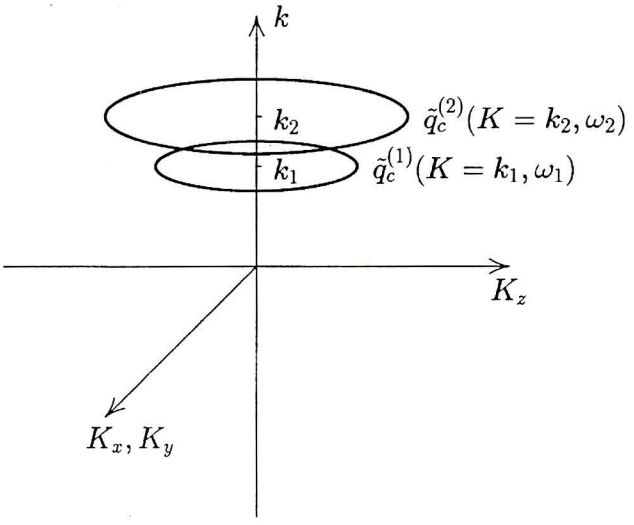

Fig. 3 - Frequency diversity in $\underline{K}$-space.

which is an explicit inversion equation with precisely defined assumption and approximations. Of course, for the angular diversity case a similar equation can be derived (Herman et al., 1987; Porter, 1986), and, instead of considering the penetrable scatterer, the prescription of perfectly soft or perfectly rigid scatterers results in inversion schemes for the "visible part" of the singular function of the scattering surface (Langenberg, 1987).

For the sake of the completeness we want to refer briefly to the monostatic case also, even though the derivation of the pertinent inversion algorithm is given in detail in (Herman et al., 1987). To obtain something like a "monostatic equivalent source" we return to the Lippmann-Schwinger equation (31) for the born approximated penetrable scatterer inserting

$$q_c^{pen,B}(\underline{\mathbf{R}}, \omega) = -k^2 F(\omega)\, O(\underline{\mathbf{R}})\, \frac{e^{jk|\underline{\mathbf{R}} - \underline{\mathbf{R}}_0|}}{4\pi\, |\underline{\mathbf{R}} - \underline{\mathbf{R}}_0|}, \tag{74}$$

where we have assumed point-source illumination from $\underline{\mathbf{R}}_0$. For the monostatic case we select $\underline{\mathbf{R}} = \underline{\mathbf{R}}_0$ to observe the scattered field and hence

$$\Phi_s(\underline{\mathbf{R}}, \omega) = -k^2 F(\omega) \iiint_{V_c} O(\underline{\mathbf{R}}')\, \frac{e^{2jk|\underline{\mathbf{R}} - \underline{\mathbf{R}}'|}}{\left(4\pi\, |\underline{\mathbf{R}} - \underline{\mathbf{R}}'|\right)^2}\, d^3\underline{\mathbf{R}}', \tag{75}$$

which gives rise to a modified scattered field

$$\Phi_s^{mo}(\underline{\mathbf{R}}, \omega) = 2\pi j \frac{\partial}{\partial k}\left[\frac{\Phi_s(\underline{\mathbf{R}}, \omega)}{k^2 F(\omega)} \right] \tag{76}$$

resulting in the differential equation

$$\Delta \Phi_s^{mo}(\underline{\mathbf{R}}, \omega) + 4k^2 \Phi_s^{mo}(\underline{\mathbf{R}}, \omega) = -O(\underline{\mathbf{R}}). \tag{77}$$

This equation defines the monostatic equivalent sources in terms of the object function itself; their field dependence has disappeared, because we already had to introduce the linearizing Born approximation in order to verify the *concept* of the equivalent sources. Equation (77) defines a Green function

$$G^{\mathrm{mo}}(\underline{\mathbf{R}}, \omega) = \frac{e^{2jk|\underline{\mathbf{R}}-\underline{\mathbf{R}}'|}}{4\pi|\underline{\mathbf{R}}-\underline{\mathbf{R}}'|}, \tag{78}$$

a pertinent Huygens principle, and the modified Porter-Bojarski integral equation for $k \geq 0$ according to

$$\psi_H^{\mathrm{mo}}(\underline{\mathbf{K}}, \omega) = \frac{\pi}{4\pi} \tilde{O}(\underline{\mathbf{K}})\, \delta(K - 2k). \tag{79}$$

Frequency diversity - the only diversity to be applied in that case - yields as inversion scheme

$$O(\underline{\mathbf{R}}) = \frac{4}{j\pi}\int_0^\infty k\, \Theta_H^{\mathrm{mo}}(\underline{\mathbf{R}}, \omega)\, dk. \tag{80}$$

2.3.3 Time Domain Backpropagation

We contain to dwell upon the monostatic case because the experimental data, which were made available to us are of that kind.

The right-hand side of (80) can be interpreted as an inverse Fourier integral with regard to frequency for $t = 0$; by definition, it involves inversion of positive frequency data only, hence, the resulting time function is complex with an imaginary part being the Hilbert transform of the real part. In order to see this explicitly we rewrite (80) introducing a unit-step function $u(\omega)$

$$O(\underline{\mathbf{R}}) = \frac{4}{\pi c^2}\int_{-\infty}^{\infty} (-j\omega)\, \Theta_H^{\mathrm{mo}}(\underline{\mathbf{R}}, \omega)\, u(\omega)\, d\omega \tag{81}$$

and realizing that its inverse Fourier transform is given by

$$F^{-1}\{u(\omega)\} = \frac{1}{2}\delta(t) + \frac{1}{2\pi j t}, \tag{82}$$

which results in

$$O(\underline{\mathbf{R}}) = \frac{4}{c^2}\left[\frac{\partial}{\partial t}\Theta_H^{\mathrm{mo}}(\underline{\mathbf{R}}, t) + j H_t\left\{\frac{\partial}{\partial t}\Theta_H^{\mathrm{mo}}(\underline{\mathbf{R}}, t)\right\}\right]_{t=0}. \tag{83}$$

Here, H_t indicates the Helbert transform with regard to t according to

$$H_t\{f(t)\} = -\frac{1}{\pi}\int_{-\infty}^{\infty} \frac{f(\tau)}{t-\tau}\, d\tau. \tag{84}$$

Per definition the object function is real valued, and, therefore,

$$H_t\left\{\frac{\partial}{\partial t}\Theta_H^{\mathrm{mo}}(\underline{\mathbf{R}}, t)\right\}_{t=0} = 0 \tag{85}$$

has to hold. Of course, this is only so for exact Born data, which leads to the conclusion that the degree of nonzeroness of the left-hand side of (85) indicates the deviation from the assumptions and approximations which are involved in the inversion scheme.

From (85), the monostatic time domain inverse scattering algorithm reads

$$O(\underline{\mathbf{R}}) = \frac{4}{c^2}\frac{\partial}{\partial t}\Theta_H^{\mathrm{mo}}(\underline{\mathbf{R}}, t)\Big|_{t=0}. \tag{86}$$

With the help of (40) we can compute $\Theta_H^{\mathrm{mo}}(\underline{\mathbf{R}}, t)$ explicitly in terms of the monostatic scattered field resulting in an exact - within the Born approximation - time domain backpropagation scheme of data to recover the object function (Herman et al., 1987).

For practical purposes it seems more appropriate to utilize some assumptions, which are in general satisfied in microwave imaging applications. First, let us evaluate (76) asymptotically for high frequencies according to

$$\Phi_s^{\mathrm{mo}}(\underline{\mathbf{R}}, \omega) \simeq \frac{2\pi j}{k^2}\frac{\partial}{\partial k}\Phi_s^I(\underline{\mathbf{R}}, \omega), \tag{87}$$

where the upper index "I" refers to "impulse response", i.e. to the $F(\omega)$ filtered field; second, we ignore the normal derivative if the data in (40) - it is hardly available except for planar and circular cylindrical measurement surfaces - and, third, we ignore terms of the order $|\underline{\mathbf{R}}-\underline{\mathbf{R}}'|^{-2}$ resulting from the normal derivative of Green's function in (40). Then we obtain from (80)

$$O(\underline{\mathbf{R}}) = \frac{4}{j\pi}\int_0^\infty dk \iint_{S_M} \frac{\partial}{\partial k}[\Phi_s^I(\underline{\mathbf{R}}', \omega)]\, \frac{e^{-2jk|\underline{\mathbf{R}}-\underline{\mathbf{R}}'|}}{|\underline{\mathbf{R}}-\underline{\mathbf{R}}'|}\, \frac{\mathbf{n}'\cdot(\underline{\mathbf{R}}-\underline{\mathbf{R}}')}{|\underline{\mathbf{R}}-\underline{\mathbf{R}}'|}\, dS', \tag{88}$$

or in time domain

$$O(\underline{\mathbf{R}}) = 4\iint_{S_M} \left(t + \frac{2|\underline{\mathbf{R}}-\underline{\mathbf{R}}'|}{c}\right) \frac{\Phi_s^I\left(\underline{\mathbf{R}}', t + \frac{2|\underline{\mathbf{R}}-\underline{\mathbf{R}}'|}{c}\right)}{|\underline{\mathbf{R}}-\underline{\mathbf{R}}'|}\, \frac{\mathbf{n}'\cdot(\underline{\mathbf{R}}-\underline{\mathbf{R}}')}{|\underline{\mathbf{R}}-\underline{\mathbf{R}}'|}\Big|_{t=0} dS'. \tag{89}$$

For closely paraxial data and image points we can further ignore the factor

$$\frac{\mathbf{n}'\cdot(\underline{\mathbf{R}}-\underline{\mathbf{R}}')}{|\underline{\mathbf{R}}-\underline{\mathbf{R}}'|}$$

to obtain

$$o(\underline{\mathbf{R}}) = \iint_{S_M} \Phi_s^I \left(\underline{\mathbf{R}}', t = \frac{2\,|\,\underline{\mathbf{R}} - \underline{\mathbf{R}}'\,|}{c} \right) dS' . \qquad (90)$$

Notice that we switched intentionally from the object function to an "image function" - it also absorbs all prefactors - because we can no longer expect that an imaging scheme relying on all the above approximations still yields the object function, or the singular function for the perfect scatterer case.

As a matter of fact, (90) is precisely the heuristic SAR time domain back-propagation scheme, which was discussed in Section 1; a fixed time sample for a fixed observation point $\underline{\mathbf{R}}'$ in data space has to be backpropagated to all image space points $\underline{\mathbf{R}}$ satisfying

$$t = \frac{2\,|\,\underline{\mathbf{R}} - \underline{\mathbf{R}}'\,|}{c} , \qquad (91)$$

which is obviously a circle. Therefore, linearized inverse scattering theory is the quantitative framework for synthetic aperture imaging.

We intensely applied and investigated the above SAR - or SAFT - scheme to nondestructive testing of materials with ultrasonic acoustic waves (Herman et al., 1987; Langenberg, 1992). But as soon as a scalar approximation of electromagnetic waves can be justified - for instance for a strictly twodimensional experimental setup -, we can utilize the same computer implementations of the algorithms as before to process microwave scattering data. Particularly, we processed data that were obtained with the measurement facility of the European Microwave Signature Laboratory of JRC in Ispra/Italy (Sieber and Nesti, 1992). The same measurements will be discussed in some more detail in (Hohmann, 1992; Nesti, 1992). Here, we simply want to illustrate the feasibility of the underlying imaging principles and their internal relationships.

The measurements comprise complex bandlimited swept frequency quasi-monostatic - transmitting and receiving antenna are separated by 29 cm - scattered field data for HH or VV polarized target illumination in either the copolarized (HH or VV) or crosspolarized (HV or VH) component; each of these components is treated as a scalar quantity. The data spectrum $\Phi_s(\underline{\mathbf{R}}, \omega)$ for positive frequencies can either be supplemented by its complex conjugate for negative frequencies to yield a real valued time function $\Phi_s(\underline{\mathbf{R}}, t)$, or we can define a complex valued time function $\Phi_s^+(\underline{\mathbf{R}}, t)$ according to

$$\Phi_s^+(\underline{\mathbf{R}}, t) = F^{-1}\{ \Phi_s(\underline{\mathbf{R}}, \omega)\, u(\omega) \}, \qquad (92)$$

that is to say, utilizing only the positive frequencies; but due to (82) we have

$$\Phi_s^+(\underline{\mathbf{R}}, t) = \frac{1}{2}\Phi_s(\underline{\mathbf{R}}, t) + j\frac{1}{2} H_t\{ \Phi_s(\underline{\mathbf{R}}, t) \}, \qquad (93)$$

which, tells us that the imaginary part is completely determined by the real part, it does not contain any new information.

Fig. 4 gives a sketch of the geometry; three cylindrical aluminum rods are distributed on an object "table" and illuminated within three frequency bands (2 -10 GHz, 10, 18 GHz, 18 - 26 GHz) from a linear aperture of width 3.4 m in a quasi-monostatic mode. Even though precise calibration (Sieber and Nesti, 1992) allows for combination of these data in a single inversione algorithm, we have chosen the 10 - 18 GHz band to compare various algorithmic alternatives. As already mentioned, we do not want to comment on the experimental details; instead, the reader is ferred to (Sieber and Nesti, 1992). Let us denote the planar measurement surface, which is actually a straight line with distance $z' = d$ from the origin, by x'. The complex time domain data $\Phi_s^+(x', z' = d, t)$ can then be processed in several ways:

1. $\Re\{ \Phi_s^+(x', z' = d, t) \} \Rightarrow o_{\Re}(x,z)$.
   We take the real part of the complex data as obtained by frequency Fourier inversion of the measurements within the 10 - 18 GHz band utilizing a Hamming window, apply the real time domain backpropagation scheme according to (90) when specialized to two spatial dimensions, and end up with a real valued image $o_{\Re}(x,z)$. Due to the frequency band limitation of the experiment this image generally exhibits an oscillatory structure, which can be suppressed complementing $o_{\Re}(x,z)$ by its Hillibert transform $H_z\{ o_{\Re}(x,z) \}$ according to

   $$o_{\Re}(x,z) + j\, H_z\{ o_{\Re}(x,z) \}$$

   to a complex image function and taking the magnitude of the latter. The result is presented as the image of Fig. 5d). The location of the three cylinders is clearly recognized; the axial resolution is proportional to the reciprocal bandwidth, the relatively poor lateral resolution is - as we assume - mostly due to the set-off of transmitter and receiver, and, of course, partly due to the finite aperture. More detailed discussions can be found in (Hohmann, 1992), addressing also the appearance of the lower amplitude ghost images as well as methods for their suppression. As a matter of fact, the ghosts originate from multiple reflections between the rods, which are not correctly handled by a linearized algorithm, which relies on the Kirchhoff approximation of physical optics.

2. $\Im\{ \Phi_s^+(x', z' = d, t) \} \Rightarrow o_{\Im}(x,z)$.

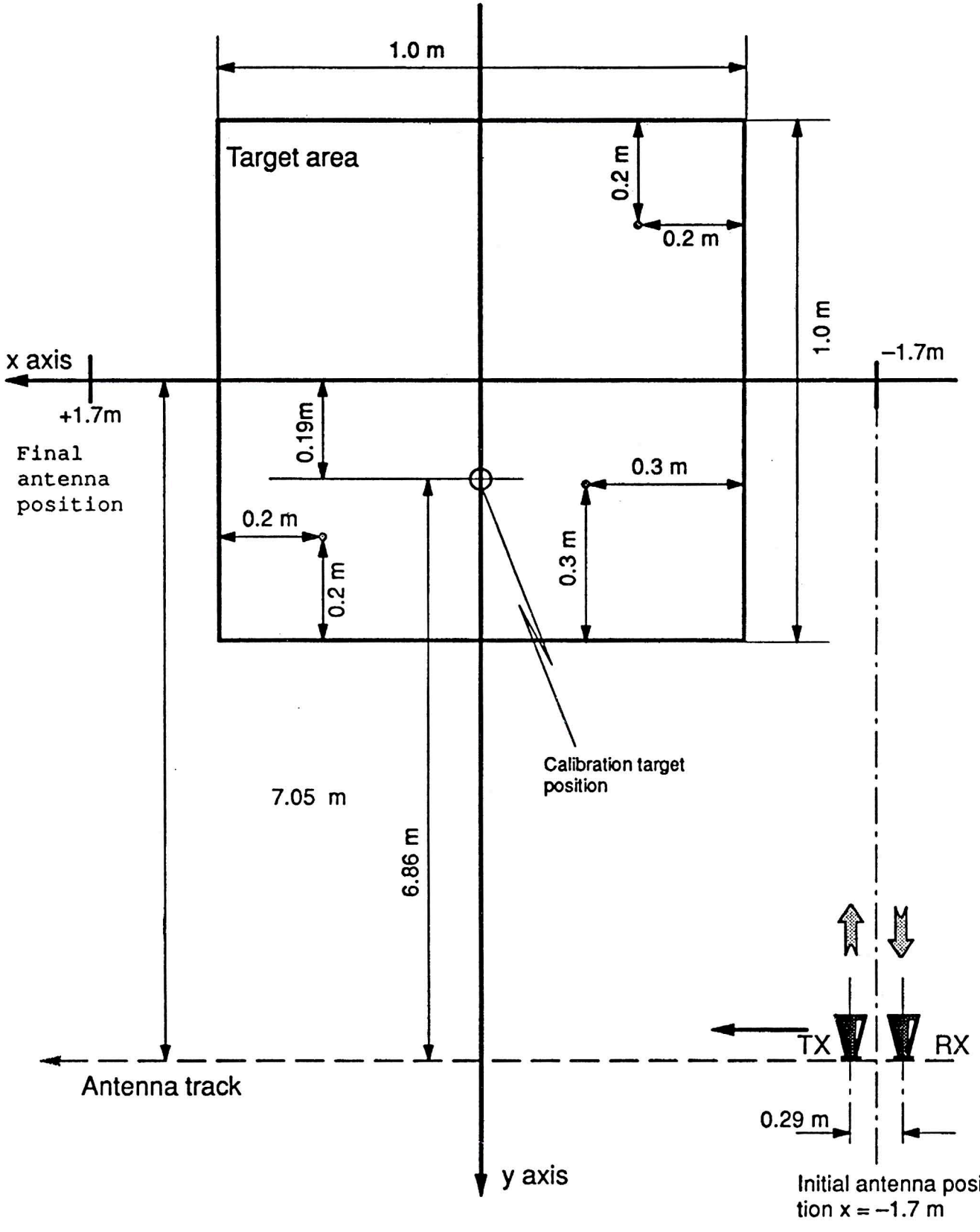

Fig. 4 - Three cylindrical rods as microwave imaging scenario.

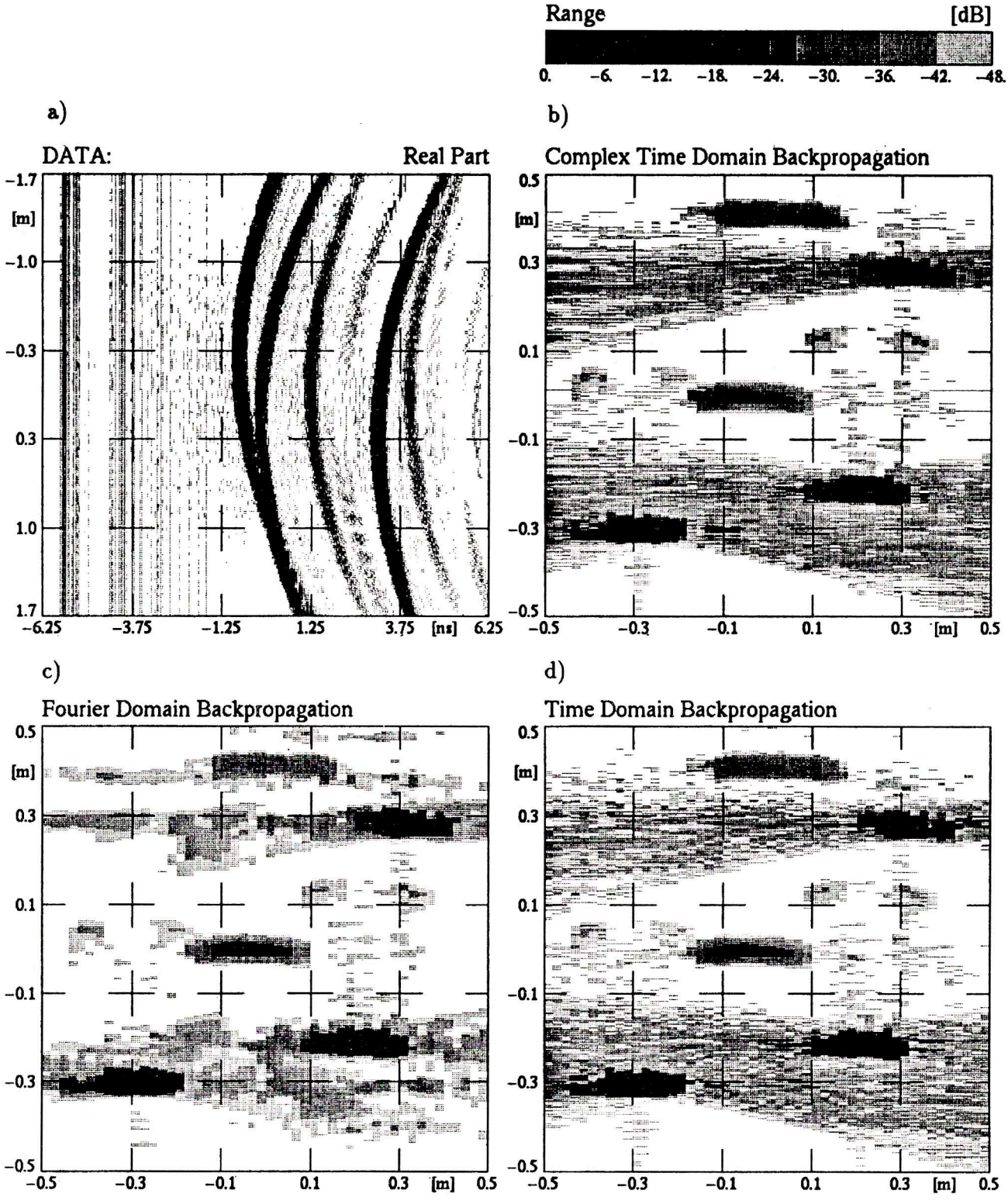

Fig. 5 - Comparison of various microwave imaging algorithms; the data in a) are given as function of time in ns and aperture coordinate in m.

We complement this imaginary part by a real part as obtained by an inverse Hillbert transform

$$H_z^{-1}\{o_{\Im}(x,z)\} + j\, o_{\Im}(x,z)$$

basically the same image results as before, i.e. we have $H_z\{o_{\Re}(x,z)\} = o_{\Im}(x,z)$, and $o_{\Re}(x,z) = H_z^{-1}\{o_{\Im}(x,z)\}$. This is shown mathematically in (Herman et al., 1987).

3. $\Phi_s^+(x', z' = d,t) \Rightarrow o_C(x,z)$.
This might be called complex time domain back-propagation; the result - the magnitude of $o_C(x,z)$ - is given as the image of Fig. 5b). Once more we observe $|o_C(x,z)| = |o_{\Re}(x,z) + j\, o_{\Im}(x,z)|$, as it is proved in (Herman et al., 1987).

Fig. 5c) displays the result of frequency diversity diffraction tomography; its discussion follows equation (109).

2.3.4 Far-field Fourier inversion

If the measurement surface is located in the far-field, it is convenient to utilize far-field data explicitly in a spatial Fourier inversion scheme. Let us once more discuss that for monostatic case - the bistatic case is dealt with in (Langenberg, 1989). The starting point is the definition of the scattering amplitude $H(\hat{\underline{\mathbf{R}}}, \omega) - \hat{\underline{\mathbf{R}}} = \underline{\mathbf{R}}/R$ - via the introduction of the far-field approximation of Green's function

$$\Phi_s^{\mathrm{mo,far}}(\underline{\mathbf{R}},\omega) = \frac{e^{2jkR}}{4\pi R}\int_{-\infty}^{+\infty}\int_{-\infty}^{+\infty}\int_{-\infty}^{+\infty} O(\underline{\mathbf{R}}')\, e^{-2jk\hat{\underline{\mathbf{R}}}\cdot\underline{\mathbf{R}}'} d^3\underline{\mathbf{R}}' = \frac{e^{2jkR}}{R} H^{\mathrm{mo}}(\hat{\underline{\mathbf{R}}}, \omega)\,. \tag{94}$$

We immediately recognize that this is nothing but the relation

$$H^{\mathrm{mo}}(\hat{\underline{\mathbf{R}}}, \omega) = \frac{1}{4\pi}\tilde{O}(\underline{\mathbf{K}} = 2k\hat{\underline{\mathbf{R}}})\,, \tag{95}$$

which says that the measurable far-field scattering amplitude is proportional to the spatial Fourier spectrum of the object function on a sphere of radius $2k$. Therefore, we can dispose measured data directly in Fourier space on the monostatic Ewald sphere. Frequency diversity then yields the complete spectral information, which is needed for the threedimensional inverse transform. For singular function type monostatic equivalent sources this procedure became well-known as the POFFIS identity (Physical Optics Far-Field Inverse Scattering) (Bojarski, 1981; Blestein, 1976). The extension to the bistatic case is discussed in (Langenberg, 1989).
With (95) we also have - compare (79) -

$$\tilde{\psi}_H^{\mathrm{mo}}(\underline{\mathbf{K}}, \omega) = \frac{\pi^2}{k} H^{\mathrm{mo}}(\hat{\underline{\mathbf{K}}}, \omega)\,, \tag{96}$$

which results in onother convenient representation of the generalized holographic field through Fourier inversion

$$\psi_H^{\mathrm{mo}}(\underline{\mathbf{R}}, \omega) = \frac{1}{8\pi k} \int_{-\infty}^{+\infty}\int_{-\infty}^{+\infty}\int_{-\infty}^{+\infty} H^{\mathrm{mo}}(\hat{\underline{\mathbf{K}}}, \omega)\, \delta(K - 2k)\, e^{j\underline{\mathbf{K}}\cdot\underline{\mathbf{R}}} d^3\underline{\mathbf{K}}\,, \tag{97}$$

if we switch to spherical coordinates, $K, \hat{\underline{\mathbf{K}}}$ in Fourier space via

$$\underline{\mathbf{K}} = K\hat{\underline{\mathbf{K}}} \tag{98}$$

yielding

$$d^3\underline{\mathbf{K}} = K^2\, dK\, d^2\hat{\underline{\mathbf{K}}} \tag{99}$$

and, therefore,

$$\psi_H^{\mathrm{mo}}(\underline{\mathbf{R}}, \omega) = \frac{k}{2\pi}\iint_{S^2} H^{\mathrm{mo}}(\hat{\underline{\mathbf{K}}}, \omega)\, e^{2jk\hat{\underline{\mathbf{K}}}\cdot\underline{\mathbf{R}}} d^2\hat{\underline{\mathbf{K}}}\,. \tag{100}$$

Here, S^2 denotes the unit-sphere. Frequency diversity of (100) with reference to (80) once more yields the far-field Fourier inversion scheme - consult again (Langenberg, 1989) for the bistatic case -, which is not surprising, if we realize by combination of (69) and (95)

$$\tilde{M}^{\mathrm{mo}}(\underline{\mathbf{K}} = 2k\hat{\underline{\mathbf{K}}}, \omega) = 4\pi H^{\mathrm{mo}}(\hat{\underline{\mathbf{K}}}, \omega)\,. \tag{101}$$

This equation means, that measurements taken on an arbitrary closed surface carry the same information as the scattering amplitude; (101) is equally valid for the bistatic case too.
In addition, (101) tells us that we can *compute* the far-field scattering amplitude form arbitrarily taken measurements in order to exploit the convenient multidimensional Fourier inversion techniques, that is to say, referring to (59) we obtain in combination with (101)

$$H^{\mathrm{mo}}(\hat{\underline{\mathbf{K}}}, \omega) = -\frac{1}{4\pi}\iint_{S_M}\left[\frac{\partial}{\partial n'}\Phi_s^{\mathrm{mo}}(\underline{\mathbf{R}}', \omega) + 2jk\,\underline{\mathbf{n}}'\cdot\hat{\underline{\mathbf{K}}}\,\Phi_s^{\mathrm{mo}}(\underline{\mathbf{R}}', \omega)\right] e^{-2jk\hat{\underline{\mathbf{K}}}\cdot\underline{\mathbf{R}}'} dS' \tag{102}$$

which might be called a near-to far-field transform; notice, in our formulation of the monostatic case there is no such thing like an incident field, whence the replacement of $\Phi(\underline{\mathbf{R}}, \omega)$ in (59) by Φ_s^{mo}.

2.3.5 Diffraction tomografy for planar measurement surfaces

Equation (102) together with (95) provides an algorithmic alternative for frequency diversity or time domain back-

propagation, as given by (80) or (86), respectively. This alternative becomes particularly attractive, if planar or circular cylindrical measurement surfaces are considered. A planar measurement surface S_M, say a plane parallel to the xy-plane of a cartesian coordinate system at distance $z = d$ from the origin, specializes (102) and (95) to the Fourier Diffraction Slice Theorem of diffraction tomography. The output of the resulting algorithm is equivalent to the time domain backpropagation scheme (SAR or SAFT), whence the name FT-SAFT for Fourier Transform SAFT, especially when applied to ultrasonic nondestructive testing. The monostatic version is discussed in detail in (Mayer et al., 1990).

Usually, the Fourier Diffraction Slice Theorem is derived from the equivalent source type representation of the scattered field, for the monostatic case (75) with (76), applying a twodimensional Fourier transform with respect to x and y (Mayer et al. 1990). An alternative results from specialization of the Porter-Bojarski integral equation to a planar surface (Herman et al., 1987). Here, we choose the most straightforward derivation writing (102)

$$H^{\mathrm{mo}}(\hat{\underline{\mathbf{K}}}, \omega) = -\frac{1}{4\pi}\int_{-\infty}^{\infty}\int_{-\infty}^{\infty}\left[\frac{\partial}{\partial z'}\Phi_s^{\mathrm{mo}}(x',y',z',\omega)\Big|_{z'=d} + 2\,j\,k\,\hat{K}_z\,\Phi_s^{\mathrm{mo}}(x',y',d,\omega)\right] e^{-2jk\hat{K}_z d} e^{-2\,j\,k\,(\hat{K}_x x' + \hat{K}_y y')}\,dx'\,dy', \tag{103}$$

where $\underline{\mathbf{n}}' = \underline{\mathbf{e}}_z$, the unit vector in z-direction; $\hat{K}_x$, $\hat{K}_y$ and $\hat{K}_z$ are cartesian components of $\hat{\underline{\mathbf{K}}}$. Obviously we have

$$\hat{K}_z = \sqrt{1 - \hat{K}_x^2 - \hat{K}_y^2}\ . \tag{104}$$

In (104), the positive sign of the square root is involved, because for observations on the plane $z = d$ the vector $\hat{\underline{\mathbf{K}}}$ points into the half-space $z \geq 0$. Defining -the factor of 2 comes from the monostatic Green's function with k replaced by $2k$ -

$$\begin{aligned} K_x &= 2k\hat{K}_x \\ K_y &= 2k\hat{K}_y \\ K_z &= \sqrt{4k^2 - K_x^2 - K_y^2} \end{aligned} \tag{105}$$

equation (103) reads

$$H^{\mathrm{mo}}(\hat{\underline{\mathbf{K}}}, \omega) = -\frac{1}{4\pi}\,e^{-jK_z d} \tag{106}$$
$$\left[\frac{\partial}{\partial z'}\int_{-\infty}^{\infty}\int_{-\infty}^{\infty}\Phi_s^{\mathrm{mo}}(x',y',z',\omega)e^{-jK_x x' - jK_y y'}\,dx'\,dy'\Big|_{z=d} + jK_z\int_{-\infty}^{\infty}\int_{-\infty}^{\infty}\Phi_s^{\mathrm{mo}}(x',y',z',\omega)e^{-jK_x x' - jK_y y'}\,dx'\,dy'\Big|_{z=d}\right],$$

where the integrals are twodimensional Fourier transforms of $\Phi^{\mathrm{mo}}(x', y', z', \omega)$ with regard to x' and y', namely

$$\hat{\Phi}_s^{\mathrm{mo}}(K_x, K_y, z', \omega) = F_{x'y'}\left\{\Phi_s^{\mathrm{mo}}(x', y', z', \omega)\right\}. \tag{107}$$

From the solution of the homogeneous equation (77), i.e. for the half-space $z \geq d$ we know

$$\frac{\partial}{\partial z'}\hat{\Phi}_s^{\mathrm{mo}}(K_x, K_y, z', \omega) = j\,K_z\,\hat{\Phi}_s^{\mathrm{mo}}(K_x, K_y, z', \omega) \tag{108}$$

and therefore, (103) becomes

$$H^{\mathrm{mo}}(\hat{\underline{\mathbf{K}}}, \omega) = \frac{1}{2\pi j}K_z\,e^{-jK_z d}\,\hat{\Phi}_s^{\mathrm{mo}}(K_x, K_y, d, \omega), \tag{109}$$

which is the monostatic Fourier Diffraction Slice Theorem. It says, that one particular sample of the twodimensional Fourier transform of data taken on a planar measurement surface with regard to the scan coordinates is proportional to the scattering amplitude in the direction $\hat{\underline{\mathbf{K}}}$, and, hence, via (95) to the object function in Fourier space at the point $\underline{\mathbf{K}} = 2\,k\,\hat{\underline{\mathbf{K}}}$; notice, evanescent wave components must be neglected because for $K_x^2 + K_y^2 > 4k^2$ the Fourier variable K_z is no longer real valued and, hence, $\underline{\mathbf{K}}$ cannot be defined. Once the Fourier space is filled through variation of $\hat{\underline{\mathbf{K}}}$ and frequency diversity, a threedimensional inverse Fourier transform yields the object function.

In (Mayer et al., 1990) we have shown explicity, that the Born case in fact requires only *one* planar measurement surface to image the *complete* object function, whereas intuitively - as well as mathematically (Mayer et al., 1990) - the singular function of a perfectly scattering surface can only be "seen" completely from two apposite planes looking at the scatterer from both sides. Even though typical targets for microwave imaging are perfectly conducting we do not give the derivation of the image quantity for one measurement plane here, because the experimental examples discussed in the following destroy the "quantitativeness" anyway due to aperture and bandwidth limitations, as well as due to the offset of trasmitting and receiving antenna, not to speak about their non-point-source-like radiation pattern and other experimental pitfalls.

Once more, the data obtained for the scenario of Fig. 4 have been under concern for processing with the algorithm as given by (109) together with (95). The twodimensional version of this algorithm is readily obtained by multiplication of (109) with $\delta(K_y)$, which is equivalent to the independence of all spatial quantities from y. Of course, the input for the Fourier Diffraction Slice theorem are complex ($\omega \geq 0$) frequency domain data; in order to perform the preprocessing as required by (87), we ignore k^{-2} within the relevant bandwidth, and evaluate the $\partial/\partial k$

- operation in the time domain by a t-multiplication. Therefore, we use $\Re\left\{\Phi_s^+(x', z' = d, t)\right\}$ as the basic input for the algorithm. The output is in general a complex valued image; it is shown as magnitude in the lower left corner of Fig. 5. Obviously, in the essential features, it does not differ from the output of the versions of time domain backpropagation, but its noise level is considerably lower. This is due to the fact, that (109) is an *exact* inversion algorithm, i.e. it implies exact spatial filtering, whereas (90) relies, as a heuristic scheme, on approximations.

2.3.6 Diffraction tomography for circular cylindrical measurement surface

As demonstrated in the last Section, (102) is extremely useful for the derivation of fast and powerful non-far field inversion algorithms. This is not only true for planar measurement surfaces but also for circular cylindrical ones, as will be shown in the following.

Considerer a circular cylindrical coordinate system r, φ, z, where the surface $r = a$ represents S_M; it encloses the scatterer completely. The outward normal in the source-point $\underline{\mathbf{R}}'$ for the integration in (102) is given by the unit-vector e'_r in radial direction; $\underline{\mathbf{R}}'$ itself has the following representation

$$\underline{\mathbf{R}}' = a\,\mathbf{e}'_r + z'\,\underline{\mathbf{e}}_z\,, \tag{110}$$

whereas for the direction $\hat{\underline{\mathbf{K}}}$

$$\hat{\underline{\mathbf{K}}} = \hat{K}_r\,\mathbf{e}_r + \hat{K}_z\,\underline{\mathbf{e}}_z \tag{111}$$

holds. Similary to (104) we have

$$\hat{K}_r = \sqrt{1 - \hat{K}_z^2}\;; \tag{112}$$

furthermore

$$\mathbf{e_r} \cdot \mathbf{e}'_r = \cos(\varphi - \varphi') \tag{113}$$

With these preliminaries we obtain from (102)

$$H^{\mathrm{mo}}(\hat{\underline{\mathbf{K}}}, \omega) = -\frac{a}{4\pi}\int_0^{2\pi}\int_{-\infty}^{\infty}\left[\frac{\partial}{\partial r'}\Phi_s^{\mathrm{mo}}(r', \varphi', z', \omega)\,\Big|_{r'=a} + \right.$$

$$\left. + 2jk\hat{K}_r\cos(\varphi - \varphi')\Phi_s^{\mathrm{mo}}(a, \varphi', z', \omega)\right] e^{-2jk[a\hat{K}_r\cos(\varphi-\varphi') + \hat{K}_z z']}\,dz'\,d\varphi'\,. \tag{114}$$

Defining

$$K_z = 2k\hat{K}_z \tag{115}$$

$$K_r = \sqrt{4k^2 - K_z^2} \tag{116}$$

reveals the z'-integration in (114) as a Fourier integral, yielding

$$H^{\mathrm{mo}}(\hat{\underline{\mathbf{K}}}, \omega) = -\frac{a}{4\pi}\int_0^{2\pi}\left[\frac{\partial}{\partial r'}\overline{\Phi}_s^{\mathrm{mo}}(r', \varphi', K_z, \omega)\,\Big|_{r'=a} + \right.$$

$$\left. + jK_r\cos(\varphi - \varphi')\,\overline{\Phi}_s^{\mathrm{mo}}(a, \varphi', K_z, \omega)\right] e^{-jaK_r\cos(\varphi-\varphi')}\,d\varphi'\,. \tag{117}$$

The overbar indicates the onedimensional Fourier transform with regard to z'.

Now we expand the monostatic Fourier transformed field $\overline{\Phi}_s^{\mathrm{mo}}(a, \varphi', K_z, \omega)$ into a Fourier series according to

$$\overline{\Phi}_s^{\mathrm{mo}}(a, \varphi', K_z, \omega) = \sum_{n=-\infty}^{\infty} a_n(K_z, \omega)\,H_n^{(1)}(K_r a)\,e^{jn\varphi'} \tag{118}$$

whit the Hankel-functions of the first kind $H_n^{(1)}$; we assume - as always - $4k^2 \geq K_z^2$, and, hence, ignore evanescent waves in z-direction. The expansion coefficients $a_n(K_z, \omega)$ are given by

$$a_n(K_z, \omega) = \frac{1}{2\pi H_n^{(1)}(K_r a)}\int_0^{2\pi}\overline{\Phi}_s^{\mathrm{mo}}(a, \varphi', K_z, \omega)e^{-jn\varphi'}\,d\varphi'\;; \tag{119}$$

they can be computed by Fourier transforming the data with regard to φ' and subsequent Hankel-function filtering with regard to the index n. A similar Fourier expansion of the exponential

$$e^{-jK_r\tau'\cos(\varphi-\varphi')} = \sum_{m=-\infty}^{\infty} J_m(K_r r')\,e^{jm(\varphi-\varphi'-\frac{\pi}{2})}\,, \tag{120}$$

taking the r'-derivate of (118) and (120) exploiting the Wronskian between Hankel-and Bessel-function J_m finally yields

$$H^{\mathrm{mo}}(\hat{\underline{\mathbf{K}}}, \omega) = \frac{1}{j\pi}\sum_{n=-\infty}^{\infty} a_n(K_z, \omega)\,e^{jn(\varphi-\frac{\pi}{2})} =$$

$$= \frac{1}{j\pi}\,\overline{\Phi}_s^{\mathrm{mo}}(a, \varphi, K_z, \omega)\,, \tag{121}$$

where $\overline{\Phi}_s^{\mathrm{mo}}(a, \varphi, K_z, \omega)$ is a φ-filtered monostatic field, which can again be computed using FFT's. With the Fourier vector

$$\underline{\mathbf{K}} = \sqrt{4k^2 - K_z^2}\,\mathbf{e_r} + K_z\,\underline{\mathbf{e}}_z\,, \tag{122}$$

equation (121) together with (95) represents the diffraction tomographic imaging scheme.

As for the planar aperture we apply the algorithm (121) to experimental data obtained by the European Microwave

Signature Laboratory at JRC (Sieber and Nesti, 1992). This time, we choose the data set for a twodimensional tree model (compare Fig. 6), which was rotated in front of fixed transmitting and receiving antennas to simulate a circular cylindrical aperture; the copolarized VV-component was as input data into (121) and (95). The image in terms of $|\, o_c\,(x\,,\,z)\,|$ is displayed in Fig. 7; the "trunk" and the "branches" of the "tree" are cleary recognized.

3. LINEAR POLARIMETRIC INVERSE SCATTERING

In general, electromagnetic wave scattering must be considered from a polarimetric point of view, and the same is true for electromagnetic inverse scattering. In particular, recently established measurement facilities (Sieber and Nesti, 1992; Blanchard et al., 1992) can provide complete polarimetric information, which should be processed in terms of appropriate algorithms. In the following, we propose such shemes extending the previously discussed scalar inverse scattering theory to the vector case; in doing so, we give only the fundametnal ideas and refer the reader to (Langenberg et al., 1992) for details.

The electric field strength satisfies the differential equation

$$[\,\nabla\nabla - (\,\nabla\cdot\nabla + k^2\,)\,\underline{\underline{\mathbf{I}}}\,]\cdot\underline{\mathbf{E}}\,(\underline{\mathbf{R}},\omega) = j\omega\mu[\,\underline{\mathbf{J}}_q\,(\underline{\mathbf{R}},\omega) + \underline{\mathbf{J}}_c\,(\underline{\mathbf{R}},\omega)\,]\,, \tag{123}$$

where $\underline{\underline{\mathbf{I}}}$ denotes the dyadic idemfactor; the inhomogeneity is composed of the prescribed source current density $\underline{\mathbf{J}}_q\,(\underline{\mathbf{R}}\,,\,\omega)$, and the equivalent current density $\underline{\mathbf{J}}_c\,(\underline{\mathbf{R}}\,,\,\omega)$ accounting for the scatterer, μ is the permeability of the host medium. Equation (123) definies a dyadic Green function

$$\underline{\underline{\mathbf{G}}}\,(\underline{\mathbf{R}} - \underline{\mathbf{R}}'\,,\,\omega) = \left(\underline{\underline{\mathbf{I}}} + \frac{1}{k^2}\,\nabla\nabla\right) G\,(\underline{\mathbf{R}} - \underline{\mathbf{R}}'\,,\,\omega) \tag{124}$$

yielding the solution

$$\underline{\mathbf{E}}_s\,(\underline{\mathbf{R}},\omega) = j\omega\mu\int_{-\infty}^{+\infty}\int_{-\infty}^{+\infty}\int_{-\infty}^{+\infty}\underline{\mathbf{J}}_c\,(\underline{\mathbf{R}}',\omega)\cdot\underline{\underline{\mathbf{G}}}\,(\underline{\mathbf{R}} - \underline{\mathbf{R}}',\omega)\,d^3\underline{\mathbf{R}}' \tag{125}$$

for the scattered field outside $V_c \bigcup S_c$; equivalently,

$j_{S_q}\,(\underline{\mathbf{R}}\,,\,\omega)$ defines an incident field $\underline{\mathbf{E}}_i\,(\underline{\mathbf{R}}\,,\,\omega)$.

Specializing to a perfecly conducting scatterer - the case of the dielectric scatterer is treated in (Langenberg et al., 1992) - we have

$$\underline{\mathbf{J}}_c\,(\underline{\mathbf{R}}\,,\,\omega) = \gamma\,(\underline{\mathbf{R}})\,\underline{\mathbf{n}}\times\underline{\mathbf{H}}\,(\underline{\mathbf{R}}\,,\,\omega) \tag{126}$$

with the magnetic field strength $\underline{\mathbf{H}}\,(\underline{\mathbf{R}}\,,\,\omega)$; insertion into (125) yields

$$\underline{\mathbf{E}}_s\,(\underline{\mathbf{R}},\omega) = j\omega\mu\iint_{S_c}[\,\underline{\mathbf{n}}'\times\underline{\mathbf{H}}\,(\underline{\mathbf{R}}'\,,\,\omega)\,]\cdot\underline{\underline{\mathbf{G}}}\,(\underline{\mathbf{R}}' - \underline{\mathbf{R}}',\omega)\,dS'\,, \tag{127}$$

which is the Huygens-type representation

$$\underline{\mathbf{E}}_s\,(\underline{\mathbf{R}}\,,\,\omega) = \iint_{S_c}\{\,j\,\omega\,\mu\,[\,\underline{\mathbf{n}}'\times\underline{\mathbf{H}}\,(\underline{\mathbf{R}}'\,,\,\omega)\,]\cdot\underline{\underline{\mathbf{G}}}\,(\underline{\mathbf{R}} - \underline{\mathbf{R}}'\,,\,\omega) + [\,\underline{\mathbf{n}}'\times\underline{\mathbf{E}}\,(\underline{\mathbf{R}}'\,,\,\omega)\,]\cdot\nabla'\times\underline{\underline{\mathbf{G}}}\,(\underline{\mathbf{R}} - \underline{\mathbf{R}}'\,,\,\omega)\,\}\,dS' \tag{128}$$

of the field for the boundary condition

$$\underline{\mathbf{n}}'\times\underline{\mathbf{E}}\,(\underline{\mathbf{R}}'\,,\,\omega) \equiv 0 \text{ for } \underline{\mathbf{R}}' \in S_c\,. \tag{129}$$

Linearization in terms of the physical optics or Kirchhoff approximation requires, that surface currents were excited as if the scattering surface was planar and infinitely large

$$\underline{\mathbf{J}}_c^{\,\mathrm{PO}}\,(\underline{\mathbf{R}}\,,\,\omega) = \begin{cases} 2\gamma\,(\underline{\mathbf{R}})\,\underline{\mathbf{n}}\times\underline{\mathbf{H}}_i\,(\underline{\mathbf{R}}\,,\,\omega) & \text{on the illuminated side} \\ 0 & \text{on the shadow side} \end{cases} \tag{130}$$

For an arbitrarily linear polarized plane wave in the direction $\hat{\underline{\mathbf{E}}}_0$ as incident field wave

$$\underline{\mathbf{E}}_i\,(\underline{\mathbf{R}}\,,\,\omega) = \hat{\underline{\mathbf{E}}}_0\,F\,(\omega)\,e^{\,j\,k\,\hat{\mathbf{K}}_i\cdot\underline{\mathbf{R}}}\,, \tag{131}$$

whence

$$\underline{\mathbf{J}}_c^{\,\mathrm{PO}}\,(\underline{\mathbf{R}}\,,\,\omega) = \frac{2\,F\,(\omega)}{Z}\,\{\,\hat{\mathbf{k}}_i\,[\,\gamma_u\,(\underline{\mathbf{R}})\cdot\hat{\underline{\mathbf{E}}}_0\,] - \hat{\underline{\mathbf{E}}}_0\,[\,\gamma_u\,(\underline{\mathbf{R}})\cdot\hat{\mathbf{k}}_i\,]\,\}\,e^{\,j\,k\,\hat{\mathbf{K}}_i\cdot\underline{\mathbf{R}}} = F\,(\omega)\,e^{\,j\,k\,\hat{\mathbf{K}}_i\cdot\underline{\mathbf{R}}}\,\underline{\mathbf{J}}_c\,(\underline{\mathbf{R}})\,; \tag{132}$$

here, the vector singular function $\gamma_u\,(\underline{\mathbf{R}})$ accounts for the shadow boundary in terms of

$$\gamma_u\,(\underline{\mathbf{R}}) = \gamma\,(\underline{\mathbf{R}})\,\underline{\mathbf{n}}\,u\,(-\hat{\mathbf{K}}_i\cdot\underline{\mathbf{n}})\,, \tag{133}$$

where $u\,(\cdot)$ is the unit-step function, Z is the wave impedance of the host medium.

Our goal is to determine the frequency independent quantity $\underline{\mathbf{J}}_c\,(\underline{\mathbf{R}})$ from appropriate, measurements on a measurement surface S_M; by definition it localizes the scattering surface, and its spatial distribution on that surface is a quantity with physical relevance.

As before we define a generalized holographic field, which, according to the representation (128), should be a vector holographic field:

$$\underline{\Psi}_H^{\mathbf{E}}\,(\underline{\mathbf{R}},\omega) = \iint_{S_M}\{\,j\,\omega\mu[\,\underline{\mathbf{n}}'\times\underline{\mathbf{H}}_s\,(\underline{\mathbf{R}}',\omega)\,]\cdot\underline{\underline{\mathbf{G}}}_i\,(\underline{\mathbf{R}} - \underline{\mathbf{R}}',\omega) + [\,\underline{\mathbf{n}}'\times\underline{\mathbf{E}}_s\,(\underline{\mathbf{R}}'\,,\,\omega)\,]\cdot\nabla'\times\underline{\underline{\mathbf{G}}}_i\,(\underline{\mathbf{R}} - \underline{\mathbf{R}}'\,,\,\omega)\,\}\,dS'\,. \tag{134}$$

With the aid of vector Green's theorem we arrive at the polarimetric counterpart of the Porter-Bojarski equation

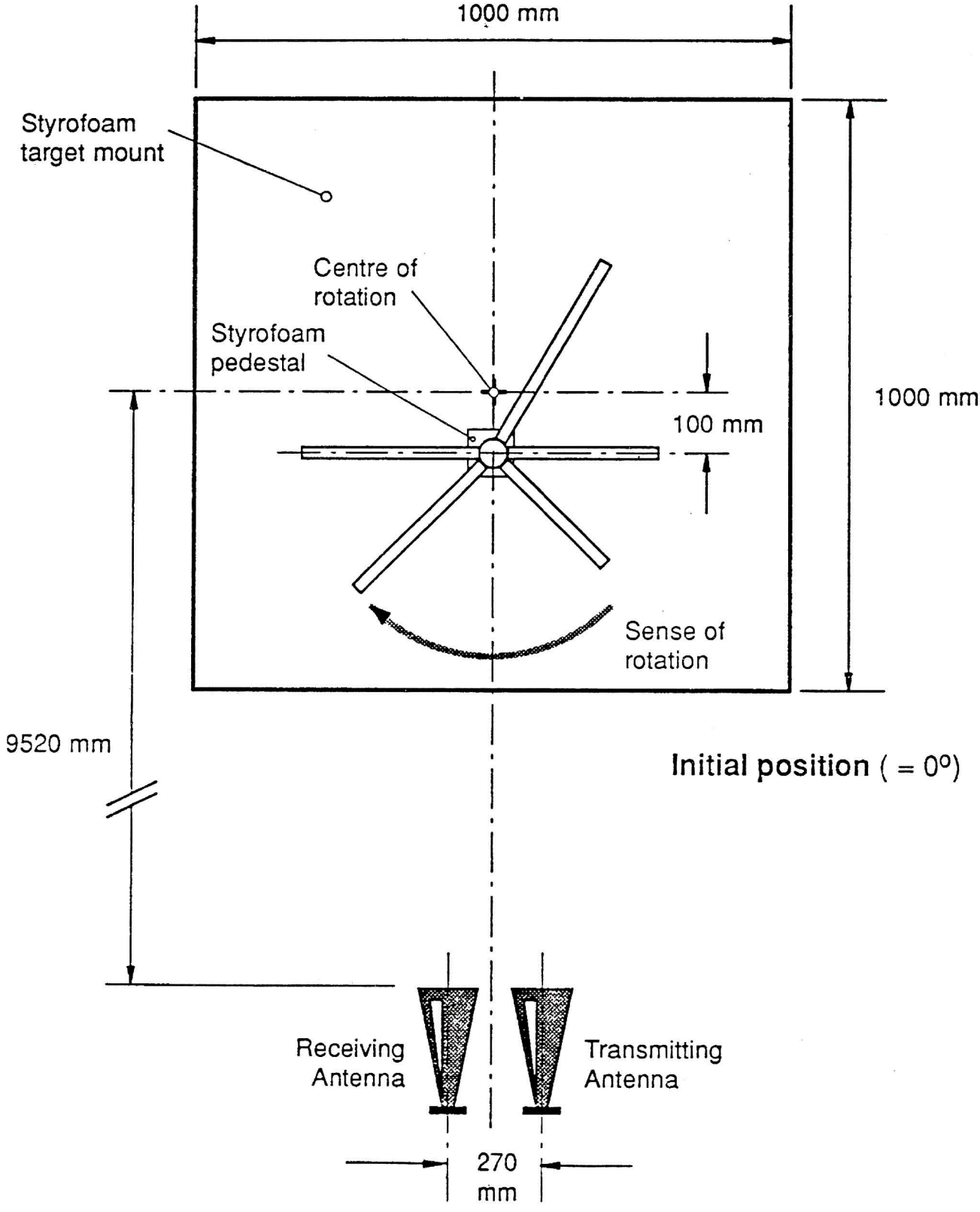

Fig. 6 - Twodimensional tree model as microwave imaging scenario.

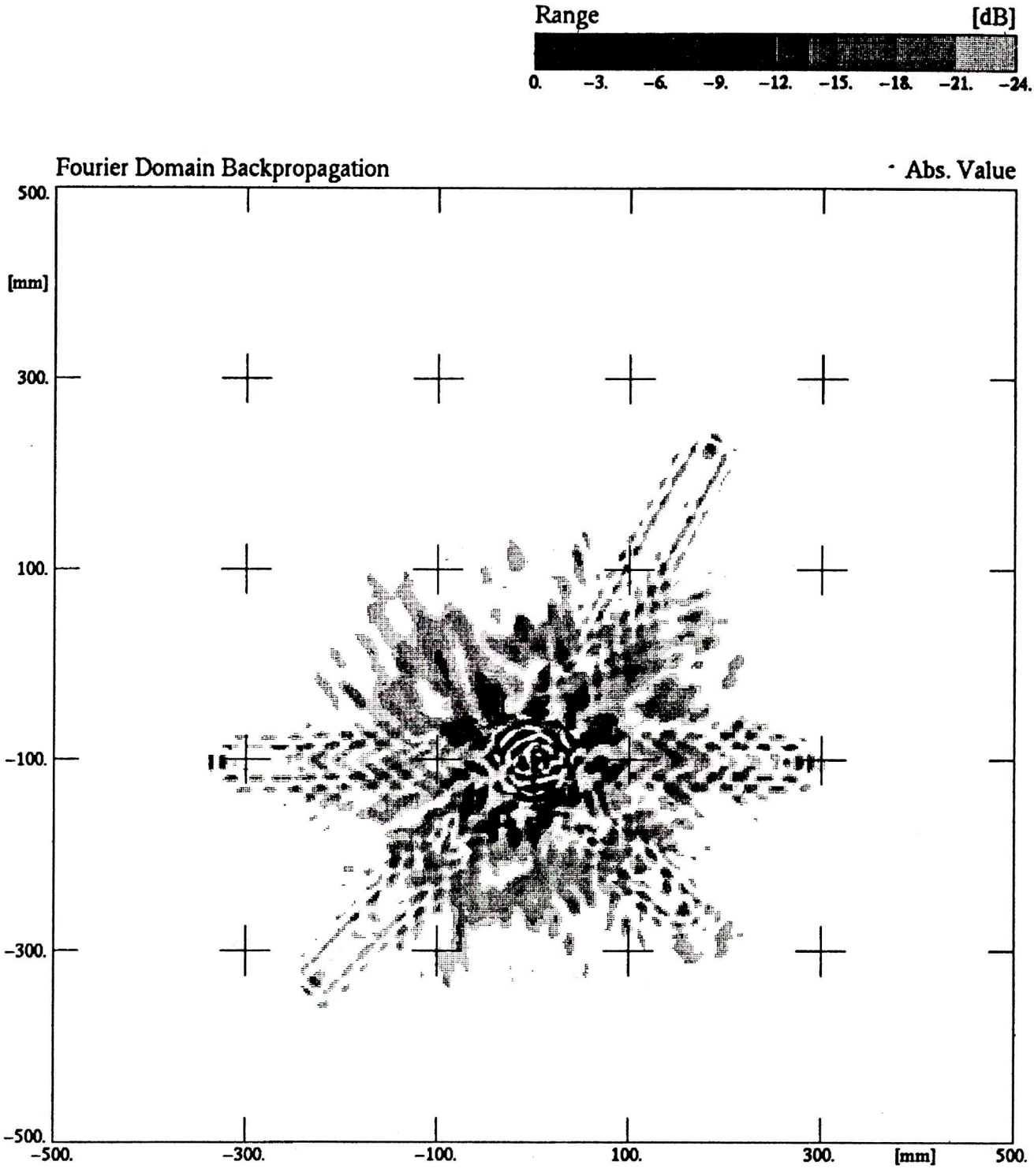

Fig. 7 - Microwave image of the twodimensional tree model of Fig. 6 as obtained with diffraction tomography for circular cylindrical apertures.

$$\underline{\Phi}_H^{\underline{E}}(\underline{R},\omega) =$$

$$j\omega\mu\int_{-\infty}^{+\infty}\int_{-\infty}^{+\infty}\int_{-\infty}^{+\infty}\underline{J}_c(\underline{R}',\omega)\cdot\underline{\underline{G}}_i(\underline{R}-\underline{R}',\omega)\,d^3\underline{R}'\,; \tag{135}$$

the upper index "$\underline{E}$" in (134) indicates that we started from the electric field Huygens-type representation. For $k \geq 0$ we have

$$\underline{\underline{G}}_i(\underline{K},\omega) = \left(\underline{\underline{I}} - \frac{1}{k^2}\underline{KK}\right)\frac{\pi}{2k}\,\delta(K-k) \tag{136}$$

and, hence, frequency diversity is again appropriate to solve (135) within the physical optics approximation. The particular problem arising in the polarimetric case concerns the inversion of the dyadic operation on $\underline{J}_c(\underline{R})$, because the determinant of $\underline{\underline{G}}_i(\underline{K},\omega)$ is zero on the Ewald sphere, therefore, sweeping Ewald spheres make it identically zero. A remedy is discussed in detail in (Langenberg et al., 1992); it consists of combining suitable projections of (135) onto known directions. A look at (132) reveals that $\hat{\underline{k}}_i$ as well as $\hat{\underline{E}}_0$ are possible candidates for such directions, and, in fact, dot multiplication of (135) with $\hat{\underline{k}}_i$ and $\hat{\underline{E}}_0$ solves our inversion problem after some dyadic manipulations, as well as extensive use of singular function properties.

The result is the following:

$$\underline{J}_c(\underline{R}) = \tag{137}$$
$$\frac{2}{Z}\Re\left\{\hat{\underline{k}}_i\,\hat{\underline{k}}_i\cdot\underline{X}(\underline{R}) - 2\,\hat{\underline{E}}_0\,\hat{\underline{k}}_i\cdot\left[F_{\underline{K}}^{-1}\left\{\underline{\hat{K}\hat{K}}\right\}\bigstar\underline{X}(\underline{R})\right]:\right.$$
$$\left.:(\hat{\underline{k}}_i\,\hat{\underline{E}}_0 - \hat{\underline{E}}_0\,\hat{\underline{k}}_i)\right\};$$

here, $\underline{X}(\underline{R})$ denotes the frequency integrated vector holographic field according to

$$\underline{X}(\underline{R}) = \frac{j}{4\pi}\int_0^{\infty}\frac{1}{F(\omega)}\underline{\Psi}_{\underline{H}}^{\underline{E}}(\underline{R},\omega)\,e^{-jk\hat{\underline{k}}_i\cdot\underline{R}}\,dk\,. \tag{138}$$

Equation (137) is an explicit reconstruction equation not only for the surface distribution of the equivalent current density, but also for the scattering geometry itself, because $\underline{J}_c(\underline{R})$ exhibits a "distributional delta-peak" on that surface; it can be numerically evaluated in various ways (Langenberg et al., 1992). Simulations for a perfeclty conducting sphere not only clearly demonstrate the feasability if this inversion scheme (Langenberg et al., 1992), but also its superiority to a pure scalar inversion algorithm applied to any component of the electric field vector.

In (Langenberg et al., 1992) we have also given an inversion equation for the object function of a dielectric - penetrable - scatterer within the Born approximation.

4. NONLINEAR INVERSE SCATTERING

Several approaches have been proposed to solve the multidimensional inverse scattering problem quantitatively, i.e. to solve the *nonlinear* inverse problem for penetrable scatterers; particularly, seriously obtained numerical results are reported in (Schüller and Chaloupka, 1989; Wang and Chew, 1989; Joachimowicz et al., 1991). In principle, one always has to cope with the non-approximated Lippmann-Schwinger equation, and the most straightforward way is its discretization with subsequent iterative solution, because it involves two unknowns, the interior field *and* the object function. Even though this procedure "works" in principle for a single-frequency-single-incident-field set up, the result would only be the minimal norm solution of generalized holography. Therefore, in contrast to the statement made in (Caorsi et al., 1991), diversity is mandatory.

In the following we give a brief discussion of our own approach, which presently relies - in contrast to (Schüller and Chaloupha, 1989; Wang and Chew, 1989; Joachimowicz at al., 1991) - solely on frequency diversity for a fixed plane wave incident field, where, additionally, access to measurements is only from "one side", i.e. we are concerned with a planar measurement surface.

We return to the scalar formulation of inverse scattering for the penetrable target and start with equation (33), which we write as

$$\Phi_i(\underline{R},\omega) = \tag{139}$$
$$\iiint_V \Phi(\underline{R}',\omega)\,[\delta(\underline{R}-\underline{R}') + k^2 O(\underline{R}')\,G(\underline{R}-\underline{R}',\omega)\,]d^3\underline{R}'\,.$$

Here, $\underline{R}$ and $\underline{R}'$ are assumed to vary in the volume $V \supset V_c$, which is discretized by N cubic cells of volume Δ^3. Considering the field as well as the object function as constant within each cell we have the approximation

$$\Phi(\underline{R},\omega) = \sum_q \phi_q(\omega)\,\Gamma_C(\underline{R}-\underline{R}_q) \tag{140}$$

$$O(\underline{R}) = \sum_p O_p\,\Gamma_C(\underline{R}-\underline{R}_p)\,, \tag{141}$$

where $\underline{R} \in V$, and $\Gamma_C(\underline{R}-\underline{R}_n)$ is the characteristic function of a single cell centered at $\underline{R}_n \in V$; hence, we have

$$\Gamma_C(\underline{R}_q - \underline{R}_n) = \delta_{q\,n} \tag{142}$$

$$\iiint_V \Gamma_C(\underline{R}'-\underline{R}_q)\,\Gamma_C(\underline{R}'-\underline{R}_p)\,d^3\underline{R}' = \Delta^3\,\delta_{q\,p}\,. \tag{143}$$

Equations (140) and (141) represent a multidimensional pulse basis function expansion with expansion coefficients $\phi_q(\omega)$ and O_p; the latter ones should be the output of an inversion algorithm: Insertion into (139) specifyng $\underline{R} = \underline{R}_n$ yields

$$\Phi_i(\underline{\mathbf{R}}_n, \omega) = \sum_q \phi_q(\omega) \tag{144}$$

$$\left[\delta_{q\,n} + k^2 O_q \iiint_{V_q} G(\underline{\mathbf{R}}_n - \underline{\mathbf{R}}', \omega)\, d^3 \underline{\mathbf{R}}' \right] =$$

$$g(\underline{\mathbf{R}}_n - \underline{\mathbf{R}}_q, \omega) = g_{n\,q}(\omega)$$

From now on, we restrict ourselves to two spatial dimensions, i.e. we have

$$G(\underline{\mathbf{R}} - \underline{\mathbf{R}}', \omega) = \frac{j}{4} H_0^{(1)}(k\,|\,\underline{\mathbf{R}} - \underline{\mathbf{R}}'\,|)\,.$$

Approximating the V_q-integration in (144) by

$$g(\underline{\mathbf{R}}_n, \omega) \simeq \frac{j}{4} \int_0^{\Delta_c} \int_0^{2\pi} H_0^{(1)}(k\,|\,\underline{\mathbf{R}}_n - \underline{\mathbf{R}}'\,|)\, d^2 \underline{\mathbf{R}}' \tag{145}$$

- it is $\Delta_c = \Delta/\sqrt{\pi}$ - we obtain according to (Richmond, 1965)

$$g(\underline{\mathbf{R}}_n, \omega) = \begin{cases} \frac{j}{2}\left[\frac{\pi \Delta_c}{k} H_1^{(1)}(k \Delta_c) + \frac{2j}{k^2} \right] & \text{for } R_n = 0 \\ \frac{j}{2} \frac{\pi \Delta_c}{k} J_1(k \Delta_c)\, H_0^{(1)}(k R_n) & \text{for } R_n > \Delta_c \end{cases}, \tag{146}$$

yielding

$$g_{n\,q}(\omega) = \tag{147}$$

$$= \begin{cases} \frac{j}{2}\left[\frac{\pi \Delta_c}{k} H_1^{(1)}(k \Delta_c) + \frac{2j}{k^2} \right] & \text{for } \underline{\mathbf{R}}_n - \underline{\mathbf{R}}_q\,| = 0 \\ \frac{j}{2} \frac{\pi \Delta_c}{k} J_1(k \Delta_c)\, H_0^{(1)}(k\,|\,\underline{\mathbf{R}}_n - \underline{\mathbf{R}}_q\,|) & \text{for } |\,\underline{\mathbf{R}}_n - \underline{\mathbf{R}}_q\,| > \Delta_c \end{cases},$$

Notice, all main diagonal elements of the matrix $g_{n\,q}(\omega)$ are equal.

If we define the following $[N \times N]$ - dimensional matrices

$$\underline{\Phi}_i(\omega) = [\,\Phi_i(\underline{\mathbf{R}}_n, \omega)\,]_{[N \times 1]} \tag{148}$$

$$\underline{\Phi}(\omega) = [\,\phi_q(\omega)\,]_{[N \times 1]} \tag{149}$$

$$\underline{\underline{\mathbf{g}}}(\omega) = k^2\,[\,g_{nq}(\omega)\,]_{[N \times N]} \tag{150}$$

$$\underline{\underline{\mathbf{O}}} = [\,O_p\, \delta_{p\,l}\,]_{[N \times N]} \tag{151}$$

equation (144) reads

$$\underline{\Phi}_i(\omega) = [\,\underline{\underline{\mathbf{I}}} + \underline{\underline{\mathbf{g}}}(\omega) \cdot \underline{\underline{\mathbf{O}}}\,] \cdot \underline{\Phi}(\omega)\,. \tag{152}$$

Its inversion

$$\underline{\Phi}(\omega) = [\,\underline{\underline{\mathbf{I}}} + \underline{\underline{\mathbf{g}}}(\omega) \cdot \underline{\underline{\mathbf{O}}}\,]^{-1} \cdot \underline{\Phi}_i(\omega) \tag{153}$$

is a matrix formulation of the direct scattering problem for the interior field.

Now we use the Lippmann-Schwinger equation to relate measurements to the interior field and to the object function

$$\Phi_s^M(\underline{\mathbf{R}}, \omega) = \tag{154}$$

$$- k^2 \iiint_V O(\underline{\mathbf{R}}')\, \Phi(\underline{\mathbf{R}}', \omega)\, G(\underline{\mathbf{R}} - \underline{\mathbf{R}}', \omega)\, d^3 \underline{\mathbf{R}}'\,.$$

Discretizing as before and specifying measurements points $\underline{\mathbf{R}} = \underline{\mathbf{R}}_m$ results in

$$\Phi_s^M(\underline{\mathbf{R}}_m, \omega) = - k^2 \sum_q \phi_q(\omega)\, O_q\, g_{m\,q}(\omega)\,, \tag{155}$$

which reads in matrix notation

$$\underline{\Phi}_s^M = \underline{\underline{\mathbf{C}}} \cdot \underline{\mathbf{O}}\,, \tag{156}$$

where

$$\underline{\Phi}_s^M = [\,\Phi_s^M(\underline{\mathbf{R}}_m, \omega_\omega)\,]_{[M\,W \times 1]} \tag{157}$$

$$\underline{\mathbf{O}} = [\,O_q\,]_{[N \times 1]} \tag{158}$$

$$\underline{\underline{\mathbf{C}}} = - k^2\,[\,\phi_q\, g_{m\,q}(\omega_\omega)\,]_{[M\,W \times N]}\,, \tag{159}$$

if we account for ω-discretized frequency diversity. The $\underline{\underline{\mathbf{C}}}$-matrix contains the field-coefficients ϕ_q, which can be computed with the help of (153). While $\underline{\mathbf{O}}$ is real valued, $\underline{\Phi}_s^M$ as well as $\underline{\underline{\mathbf{C}}}$ are complex, hence, (159) is twofold overdetermined if $M\,W = N$. In addition, $\underline{\underline{\mathbf{C}}}$ is ill-conditioned, and consequently, the inversion of (159) has to be regularized. We apply the Phillips-Tikhonov tecnique, and solve

$$(\underline{\underline{\mathbf{C}}}^+ \cdot \underline{\underline{\mathbf{C}}} + \lambda\, \underline{\underline{\mathbf{I}}}) \cdot \underline{\mathbf{O}} = \underline{\underline{\mathbf{C}}}^+ \cdot \underline{\Phi}_s^M \tag{160}$$

instead of (159); here, $\underline{\underline{\mathbf{C}}}^+$ denotes the adjoint of $\underline{\underline{\mathbf{C}}}$. The regularization parameter λ is adaptively chosen for each iteration step according to (Marquardt, 1963; Habashy et al., 1990)

$$\lambda = \alpha \frac{||\,\underline{\Phi}_s^{M,\,meas} - \underline{\Phi}_s^{M,\,calc}\,||}{||\,\underline{\Phi}_s^{M,\,meas}\,||}\,, \tag{161}$$

where α is an arbitrary factor, and $\underline{\Phi}_s^{M,\,calc}$ is the calculated output of (153), while $\underline{\Phi}_s^{M,\,meas}$ stands for the measured (or simulated) data; $||\cdot||$ is the norm induced by the scalar product. This way, λ can be reduced for each more and more well-posed iteration step ensuring "smoother" convergence. For the first iteration, we use the incident field to compute $\underline{\underline{\mathbf{C}}}$ in (160), i.e. we apply the Born approximation, and λ is chosen "free-handedly". The resulting $\underline{\mathbf{O}}$ is utilized to compute the total field in V for all frequencies applying (153); this field and this object function enters (156) to produce $\underline{\Phi}_s^{M,\,calc}$, and a new regularization parameter emerges from (161). Fig. 8 illustrates the iteration through a flow-chart.

To invert (160) most effectively, the conjugate gradient technique is applied minimizing the least square error for the matrix equation

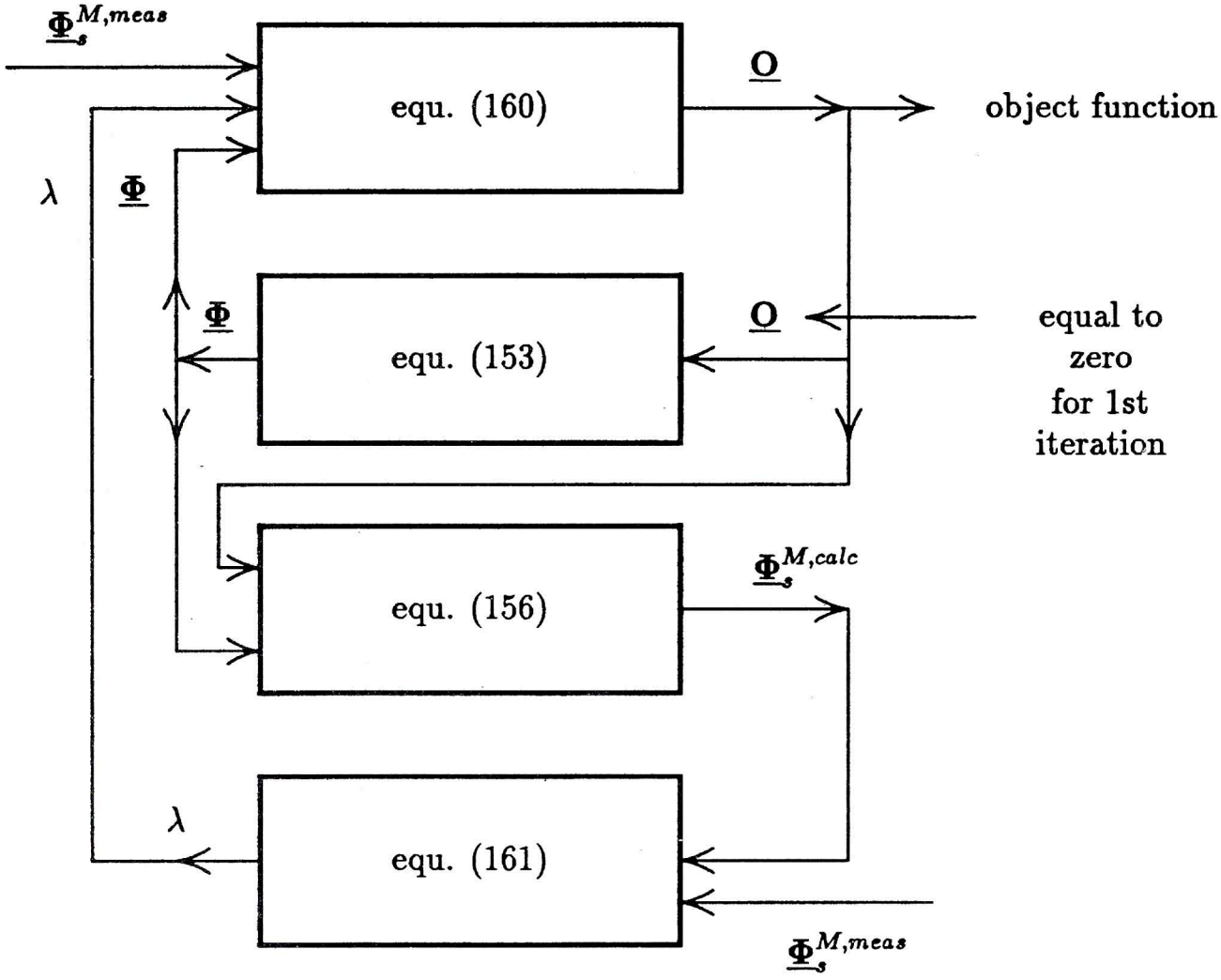

Fig. 8 - Flow-chart for nonlinear iterative inverse scattering.

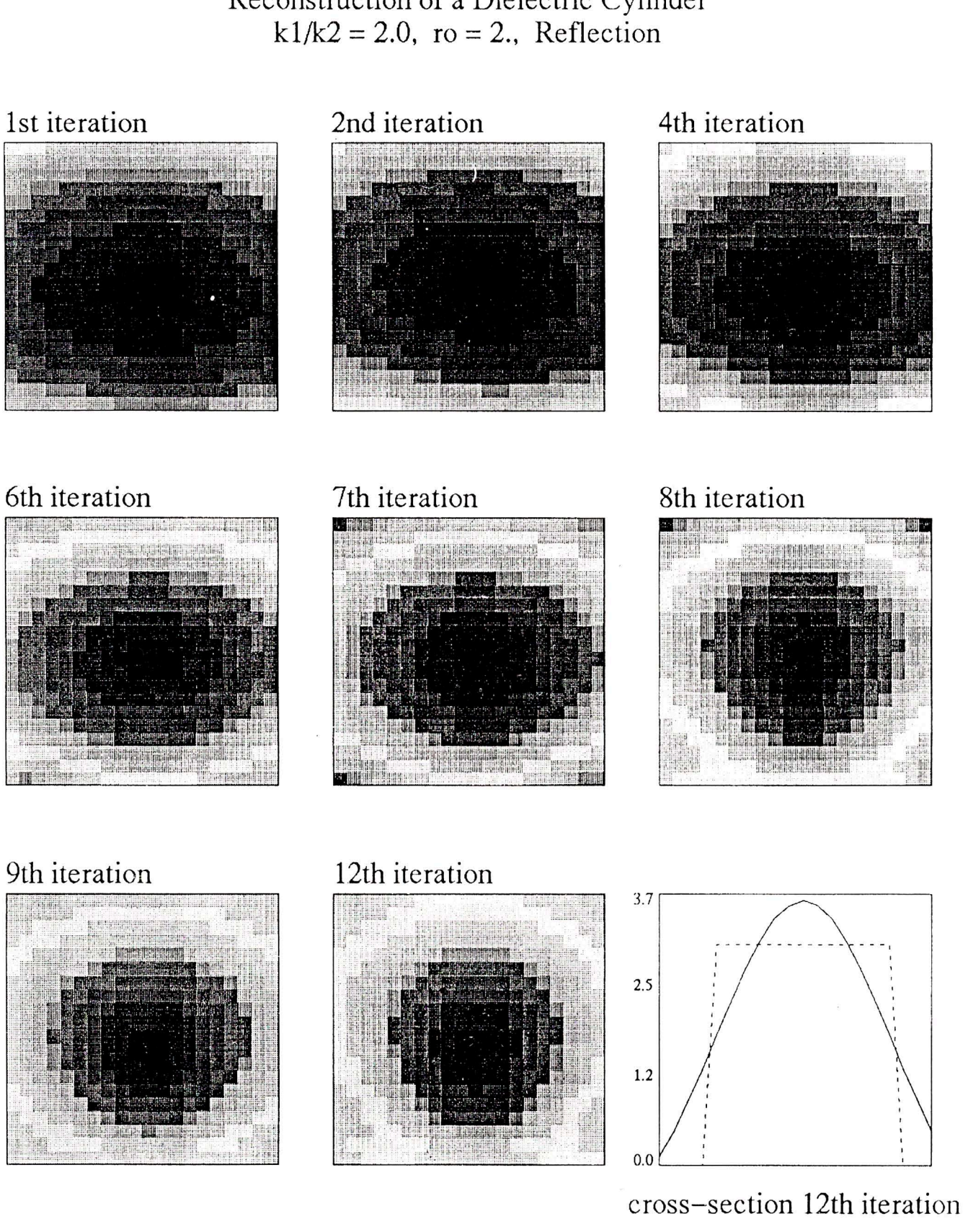

Fig. 9 - Simulation results for nonlinear iterative scattering. A circular cylinder a is centered within a square discrezation area of size $20\,\Delta \times 20\,\Delta$ *with* $20\,\Delta = 3\,a$ *. In the lower right corner, the cross-section of the result of the 12th iteration is shown and compared to the cylender cross-section in terms of the object function.*

$$\underline{\underline{\mathbf{A}}} \cdot \underline{\mathbf{O}} - \underline{\mathbf{d}} = \underline{\mathbf{a}} \tag{162}$$

with the residual $\underline{\mathbf{a}}$, and

$$\underline{\underline{\mathbf{A}}} = \begin{pmatrix} \Re\, \underline{\underline{\mathbf{C}}} \\ \Im\, \underline{\underline{\mathbf{C}}} \\ \sqrt{\lambda}\, \underline{\underline{\mathbf{H}}} \end{pmatrix}_{[(2MW+N)\times N]} \tag{163}$$

$$\underline{\mathbf{d}} = \begin{pmatrix} \Re\, \underline{\Phi}_s^M \\ \Im\, \underline{\Phi}_s^M \\ \underline{\mathbf{o}} \end{pmatrix}_{[(2MW+N)\times 1]} \tag{164}$$

It can be shown (Louis, 1989), that minimizing (162) with (163) and (164) in the least square sense is equivalent to the solution of

$$(\underline{\underline{\mathbf{A}}}^+ \cdot \underline{\underline{\mathbf{A}}} + \lambda\, \underline{\underline{\mathbf{H}}}^+ \cdot \underline{\underline{\mathbf{H}}}) \cdot \underline{\mathbf{O}} = \underline{\underline{\mathbf{A}}}^+ \cdot \underline{\mathbf{d}} \tag{165}$$

with

$$\underline{\underline{\mathbf{A}}} = \begin{pmatrix} \Re\, \underline{\underline{\mathbf{C}}} \\ \Im\, \underline{\underline{\mathbf{C}}} \end{pmatrix}_{[(2MW)\times N]} \tag{166}$$

$$\underline{\mathbf{d}} = \begin{pmatrix} \Re\, \underline{\Phi}_s^M \\ \Im\, \underline{\Phi}_s^M \end{pmatrix}_{[(2MW)\times 1]} \tag{167}$$

to find $\underline{\mathbf{O}}$; obviously, the choice $\underline{\underline{\mathbf{H}}} = \underline{\underline{\mathbf{I}}}$ is just the zero-order Phillips-Tikhonov regularization.

Fig. 9 gives a numerical expample; as target, we have chosen a circular cylinder of radius a and wavenumber $k_1 = 2k$, centured in the "volume" V, which is discretized into 20×20 cells, and 20 frequencies within the interval $\pi/500 \le ka \le \pi/8$ have been selected; 20 "measurement points" are located on the bottom boundary of V, the plane wave illuminating the cylinder comes from that "surface" as well. Simulated data emerge from an eigenfunction expansion. Fig. 9 displays the results of various iterations in terms of the magnitude of $\underline{\mathbf{O}}$ normalized to its own maximum for the iteration under concern; we have chosen $\alpha = 2$. Obviously, the inversion procedure converges to a useful solution. Notice, frequency diversity alone and the very constrained measurement surface represent a highly ill-conditioned setup, and, therefore, we judge the results as promising for further investigation.

ACKNOWLEDGEMENTS

We highly appreciate he help of Dr. Sieber, Dr. Nesti and Mr. Hohmann from the European Microwave Signature Laboratory at JRC to provide us with experimental data as input for our microwave imaging algorithms.

REFERENCES

Blanchard, A.J., Williams B., Schindel, R.F., Jersah, B., Krenek B., 1992, The Harc holographic imaging facility - Multistatic images of distributed targets. Advances in Remote Sensing, this issue.

Bleistein, N., 1976, Physical optics far-field inverse scattering in the time domain. J. Acoust. Soc. Am, 60, 1249.

Boerner, W.M. et al. (Eds.), 1992, Direct and Inverse Methods in Radar Polarimetry (Dordrecht: Reidel).

Boerner, W.M., Yan, W.L., XI, A:Q., Yamaguchi, Y., 1991, On the basic principles of radar polarimetry: The target characteristic polarization state theory of Kennaugh, Huyne's polarization fork concept, and its extension to the partially polarized case. Proc. Ieee, 79, 1538.

Bojarski, N.N., 1981, Exact inverse scattering theory. Radio Science, 16, 1025.

Bojarski, N.N., 1982, A survey of the physical optics inverse scattering identity. Ieee Trans. Ant. Propagat., Ap-30, 980.

Caorsi, S., Gragnani, G.L., Pastorino, M., 1991, A multiview microwave imaging system for two-dimensional penetrable objects. Ieee Trans. Microwave Theory Techn., Mtt-39, 845.

Esmersoy, C., Oristaglio, M.L. Levy, B.C., 1985, Multidimensional Born velocity inversion: single wideband point source. J. Acoust. Soc. Am., 78, 1052.

Habashy, T.M., Chow, E.Y., Dudley, D.G., 1990, Profile inversion using the renormalized source-type integral equation approach. Ieee Trans. Ant. Propagat., Ap-38, 668.

Hargert, R.O., 1970, Syntethic Aperture Radar System, Theory and Design (New York: Academic Press).

Herman, G.T., Tuy, H.K., Langenberg, K.J., Sabatier, P., 1987, Basic Methods of Tomografy and Inverse Problems (Bristol: Adam Hilger).

Hohmann, M., 1992, Potential for ghosts in high resolution radar images due to multiple reflection. Advances in Remote Sensing, this issue.

Joachimowicz, N., Pichot, C., Hugonin, J.P., 1991, Inverse scattering: An iterative numerical approach for electromagnetic imaging. Ieee Trans. Ant. Propagat., Ap-39, 1742.

Keller, J.B., 1969, Accuracy and Validity of the Born and Rytov Approximation. J. Optic. Soc. Am., 59, 1003.

Langenberg, K.J., Theoretical aspects of target classification: physical optics and Radon transform methods. In: Theoretical Aspects of Target Classification. Felsen, L.B. (Ed.), 1987, Agard Lecture Series, 152.

Langenberg, K.J., 1989, Introduction to the special Issue on Inverse Problems. Wave Motion, 11, 99.

Langenberg, K.J., Elastic wave inverse scattering as applied to nondestructive evalutation. In: Inverse Problems in Scattering and Imaging. Bertero, M. (Ed.), 1992 (Bristol: Adam Hilger).

Langenberg, K.J., Brandfass M., Fellinger, P., Gurke, T., Kreutter, T., A unified theory of multidimensional electromagnetical vector inverse scattering within the Kirchhoff or Born approxi-

mation. In: Modern Problems in Radar Target Imaging. Überall, H., (Ed.), 1992, (Berlin: Springer).

Li, H.J., Lin, F.L., Shen, Y., Farhat, N.H., 1990, A generalized interpretation and prediction in microwave imaging involving frequency and angular diversity. J. Electromagnetic Waves Appl., 4, 415.

Louis, A.K., 1989, Inverse und schlecht gestellte Probleme (Stuttgart: Teubner).

Marquardt, D.W., 1963, An algorithm for least-squares estimation of nonlinear parameters. J. Soc. Industr. Appl. Math., 11, 431.

Mayer, K., Marklein, R., Langenberg, K.J., Kreutter, T., 1990, Three-dimensional imaging system based on Fourier transform syntethic aperture focusing technique. Ultrasonic, 28, 241.

Mensa, D.L., 1981, High Resolution Radar Imaging (Dedham: Artech House).

Nesti, G., 1992, Wide-band polarimetric 2D imaging of a small tree. Advances in Remote Sensing, this issue.

Oristaglio, M.L., 1989, An inverse scattering formula that uses all the data. Inverse Problems, 5, 1097.

Porter, R.P., 1970, Diffraction-limited scalar image formulation with holograms of arbitrary shape. J. Opt. Soc. Am., 60, 1051.

Porter, R.P., 1986, Scattered wave inversion for arbitrary receiver geometry. J. Acoust. Soc. Am., 80, 1220.

Richmond, J.H., 1965, Scattering by a dielectric cylinder of arbitrary cross-section shape. Ieee Trans. Ant. Propagat., Ap-13, 334.

Sieber, A.J., Nesti, G., 1992, The European Signature Laboratory - A new research facility. Advances in Remote Sensing, this issue.

Schmitz, V., Müller, W., Schäfer, G., 1986, Practical experiences with.

L-Saft. In: Review of Progress in Quantitative Nondestructive Evaluation. Thompson, D.O., Chimenti, D.E. (Eds.), 1986, (New York: Plenum Press).

Schüller, M., Chaloupka, H., 1989, Improved reconstruction in diffraction tomography by means of a nonlinear scattering model. Proc. Int. Ursi Commission B Symp. Electromagnetic Theory, Stockholm, 584.

Wang, Y.M., Chew, W.C., 1989, An iterative solution of the two-dimensional electromagnetic inverse scattering problem. Int. J. Imaging Systems and Technology, 1, 100.

Wehner, D.R., 1987, High Resolution Radar (Norwood: Artech House).

Zebker, H.A., Van Zyl, J.J., 1991, Imaging radar polarimetry: A review. Proc. Ieee, 79, 1583.